MSc Thesis : Investigation of Broadband Laser Spectral Fluctuations with Application to CARS

J.M. Horrell

January 15, 1993

Abstract

An investigation is made into the major factors contributing to shot-to-shot spectral fluctuations in a broadband dye laser with a view to reducing noise in Coherent Anti-Stokes Raman Spectroscopy (CARS). Combinations of three dyes and methods of quantifying noise in spectra are investigated. Correlations between groups of modes in the dye laser are shown to exist and vary from dye to dye. Investigation is made into the effects that the insertion of scattering particles into the dye laser oscillator has on the spectral noise. A tunable, solid state Ti:Sapphire laser is assembled and spectra obtained for comparison with the dye laser spectra.

Contents

List of Figures

List of Tables

1 Introduction

Coherent Anti-Stokes Raman Spectroscopy (CARS) is one of the most widely used nonlinear mixing spectroscopy techniques and is capable of nonintrusive major species concentration and temperature measurements with good spatial and temporal resolution. This capability makes CARS an ideal tool for analysis of turbulent combustion environments. Work carried out at the University of Cape Town (UCT) using this technique has concentrated on nitrogen gas thermometry in the utilisation of fossil fuels. Large shot-to-shot spectral fluctuations in the CARS signal have been observed at UCT and have been widely reported elsewhere [1] [2] [3] [4].

Various techniques have been developed to minimise the effect of the shot-to-shot spectral fluctuations. Where an instantaneous measurement is required, it is possible to correct the CARS spectrum with an accurate nonresonant reference spectrum (using a reference cell) which is generated simultaneously. This technique can result in some difficulties, especially in beam alignment and Pealat et al. [2] have shown that noise arising from Stokes shot-to-shot fluctuations cannot be completely eliminated in this way. Otherwise, where an instantaneous measurement is not required, averaging over a number of CARS spectra can be employed.

The second harmonic of a single longitudinal mode Nd:YAG laser is used as the pump beam and a broadband dye laser is used as the Stokes beam for CARS work at UCT. The dye laser is pumped by split-off portions of the frequency-doubled Nd:YAG. There has been some debate in the literature as to the relative noise merits of using single-mode and multimode pump lasers for CARS [5] [3] [6], however there is agreement that the shot-to-shot fluctuations in the Stokes laser are a major source of CARS noise [2]. Studies have been carried out into temporal smoothing of dye laser pulses using saturated amplification to stabilise the pulse energy [7] [8]. However, for CARS work, information is derived from the spectral shape and pulse energy stabilisation of the Stokes laser is less important than spectral fluctuations in the signal.

It is believed that the Stokes laser spectral fluctuations originate in the statistical nature of the quantum noise which is present in the laser buildup [7] [9]. This is confirmed by the theoretical analysis of Mironenko and Yudson [10] [11] which shows that the generation spectrum of a multimode laser is not smooth, but a "heavily jagged frequency function". The analysis, however, takes no account of possible correlations between modes.

Pealat et al. [2] predict that the use of Stokes lasers with improved spectral profiles should halve the uncertainty associated with CARS temperature measurements (of the order of 50 K). With the advent of tunable, solid-state, broadband lasers it should be possible to use a laser such as the $Ti^{3+} : Al_2O_3$ laser as the Stokes beam instead of the dye laser, provided potential problems associated with the build-up time can be overcome. In our laboratory, work is being performed to produce a pump beam at the correct frequency for use with the $Ti^{3+} : Al_2O_3$ laser using Backward Stimulated Raman Scattering (Backward SRS) [12].

The $Ti^{3+} : Al_2O_3$ laser is expected to show considerably reduced shot-to-shot spectral fluctuations in comparison with the dye laser as the effects of the turbulent flow of the dye and chemical interactions within the active medium are not understood and may contribute significantly to shot-to-shot spectral noise. Indeed, Chyba et al. [13] have attributed the chaos in a single-mode dye laser to the turbulent dye flow in the dye cell. Chaos was absent from two similar dye lasers which use a dye jet rather than a dye cell.

Therefore, in order to improve the CARS results it is important to investigate the factors affecting shot-to-shot spectral fluctuations of the dye laser. A qualitative measure of spectral fluctuations can be obtained by observing the trace of an oscilloscope which is connected to the detector, but a more rigorous method of quantifying shot-to-shot fluctuations is required if the performance of the dye laser is to be evaluated under varying conditions (such as using different dyes). This quantitative measure of noise is also needed for a comparison with the $Ti^{3+} : Al_2O_3$ laser.

Most published work on CARS noise and noise in multimode lasers has assumed independence of the laser modes [3] [14] [6] [10]. The rationale for this assumption as expressed by Greenhalgh and Whittley [14] is that typically $> 10^4$ modes are present in a broadband dye laser with a bandwidth of $\sim 5\ nm$ and therefore the loss of one mode has little effect on the other modes, "which leads to the important conclusion that individual modes are statistically independent".

Westling and Raymer et al. [9] [15] have shown that mode correlations as well as mode anticorrelations exist in a pulsed dye laser due to competition for the gain and spatial hole burning. This is consistent with the maximum-emission principle of Statz and Tang [16].

In an earlier paper on time autocorrelation of the total broadband output intensity of a multimode cw dye laser [17], Westling et al. have shown that at low powers only two correlated longitudinal modes lase at any time athough

the time-averaged spectrum appears fairly smooth. Above a critical power there is a transition to a "chaotic" state where many modes lase simultaneously and are uncorrelated. Further studies on the dynamical instabilities of multimode lasers using concepts such as attractor dimension from chaos theory have been performed by Atmanspacher and Scheingraber [18] as well as by Kotomtseva et al. [19].

Atmanspacher et al. [20] use a model of packets of strongly coupled modes at lower spectral powers to explain mode correlation times in a multimode cw dye laser. At higher powers the number of mode packets increases. The extension of these results to a pulsed broadband dye laser has not been investigated fully. Thus, in general, the light from a multimode laser is not well described by the model of chaotic light where mode phases and amplitudes are statistically independent.

Kröll et al. [3] state that the assumption of independent modes is expected to be valid for a pulsed dye laser operating high above threshold as, in this regime, spatial hole burning and mode competition are negligible. However, in a paper on CARS noise using a broadband dye laser as the Stokes beam [1], Snelling et al. indicate that the existence of mode correlations in the Stokes laser, reducing the number of independent modes, is the most likely explanation for their experimental results. The validity of the assumption of independent modes in a pulsed dye laser, operating high above threshold, is investigated using autocorrelation analysis in Section 5.4.

In the past, a mixture of two dyes, Rhodamin 610 (Rh610) and Rhodamin 640 (Rh640), had been used for the CARS work in this laboratory. For the nitrogen thermometry work being done, the fluorescent peak of the broadband dye laser is required at 606.7 nm. This is aiming half way between the main peak and the "hot band" and assumes a Raman frequency of $2315cm^{-1}$.

Another dye which can be diluted (with ethanol) so that it fluoresces at the required wavelength without requiring mixing with another dye is Sulforhodamin 101 (SfRh101). The dilution required, however, is at the expense of beam power and it has been found that the dye laser beam power is too low for satisfactory CARS work.

Preliminary investigation in May 1991 revealed that the SfRh101 on its own is considerably more spectrally reproducible than the Rh610/640 mixture. Initially, this led to the conclusion that the mixing dyes should be avoided. However, as the SfRh101 was unsatisfactory on its own, it was decided to mix the SfRh101 with the Rh610. This seemed a logical step as the fluorescence peaks of the SfRh101- and Rh610 dyes lie closer to each other than those of

Rh640 and Rh610. In addition, the SfRh101 had proved to be considerably less noisy than the Rh610/640 mixture.

Subsequent investigation in June 1992 revealed that the Rh610/SfRh101 mixture *was* less noisy than the Rh610/Rh640 mixture, but not by much. It was also very apparent that the June 1992 spectral measurements were, on the whole, much less noisy than those of May 1991. The only apparent difference in the experiments lay in the method of choosing the dye amplifier concentrations. The laser manufacturers recommend using a third of the oscillator concentrations in the dye laser amplifier. This seems to be an empirical rule and was used for the May 1991 measurements.

In June 1992, however, it was decided to add a third of the Rh610 concentration to the amplifier and then to tune the amplifier to the correct wavelength (606.7 nm) by adding the Rh640 or SfRh101. Thus the Rh610 or SfRh101 concentration in the amplifier would be higher than that in the oscillator.

In addition, the effects of inserting a bandpass filter into the dye laser oscillator as well as between the oscillator and amplifier, were investigated. It was found that this did not improve the spectral profiles and so the use of the filter was discontinued.

In this thesis, an attempt has been made to isolate the principal causes of dye laser spectral noise. Combinations of three dyes, Rh610, Rh640, and SfRh101, as well as methods of tuning have been investigated with an aim to produce a dye beam, suitable for CARS work, peaking at 606.7 nm. The investigation includes the aquisition of nonresonant CARS spectra from a cell containing argon, generated using the various dye combinations. The introduction of scattering particles into the dye laser oscillator has also been investigated as a possible method of reducing spectral fluctuations. Three sizes of scattering particle have been investigated as well as different particle concentrations. Finally, a broadband, tunable, solid state Ti:Sapphire laser has been assembled and spectra obtained for noise comparison with the dye laser spectra. Methods of noise characterization have been investigated and auto-correlation techniques have been used for the investigation of correlations between groups of modes in lasers.

Pealat et al. [2] indicate that a significant contribution to CARS noise is a result of the very high frequency structure with a period of the order of the dye laser mode spacing. Variations in response to the different rotational lines are caused by shot-to-shot frequency jitter and amplitude fluctuations. This very high frequency spectral noise is not addressed in the analysis of this thesis as the highest possible spectral resolution observed corresponded

to one detector pixel of the OMA. Of the order of ten longitudinal modes of the dye laser are observed with each pixel. This is not taking the effects of detector cross-talk into account, which reduce the resolution further.

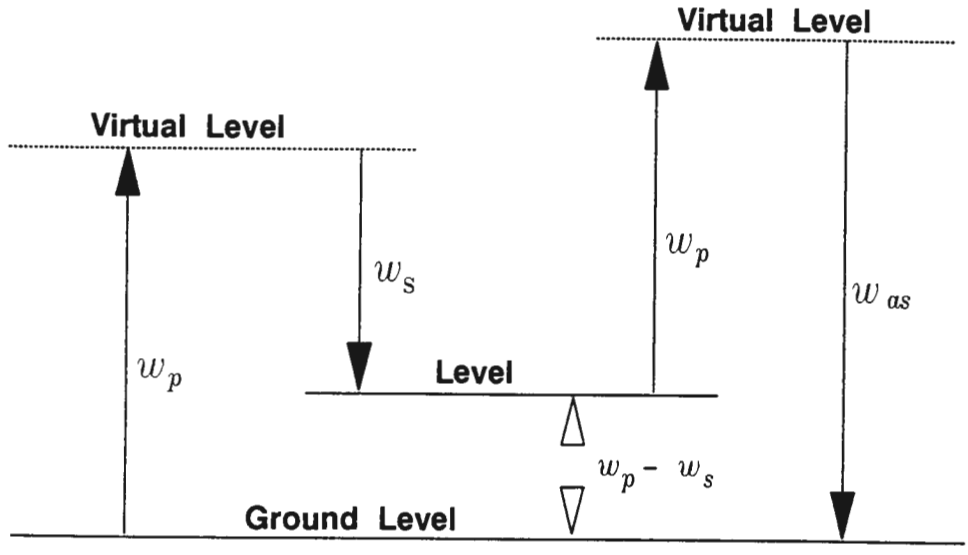

Figure 1: The CARS Interaction

2 Theory

2.1 Brief CARS Theory

In this section a brief discussion of the background theory to the CARS interaction is given. Rigorous treatments of CARS theory can be found in References [21].[22]. and [23].

CARS is a nonlinear optical process involving three-wave mixing. Laser fields at two different frequencies, ω_p and ω_s, are used to excite a medium, interacting through the third-order nonlinear electric susceptibility $\chi^{(3)}$ of the medium. A coherently oscillating polarization at a frequency corresponding to a threefold sum of the incident frequencies is produced. The resulting induced polarisation field acts as the source term in Maxwell's wave equation and a CARS beam at frequency $\omega_{as} = \omega_p + (\omega_p - \omega s)$ is produced. Figure 1 gives schematic view of the CARS interaction.

$\chi^{(3)}$ has resonant and nonresonant contributions and so the three-wave mixing occurs for all samples. If $\omega_p - \omega_s$ corresponds to a Raman transition, the

CARS beam is resonantly enhanced.

The intensity of the CARS signal which is dependent on the intensities of the pump- and Stokes beams as well as on $\chi^{(3)}$ is given by

$$I_{as} \propto |\chi^{(3)}|^2 I_p^2 I_s \tag{1}$$

where I_{as}, I_p and I_s denote the intensities of the CARS, pump, and Stokes beams, respectively. Thus it is clear that shot-to-shot spectral fluctuations in the Stokes beam result in spectral fluctuations in the CARS signal.

2.2 Theory of Broadband Laser Radiation

In this section, a model of broadband laser radiation describing temporal and spectral fluctuations, is presented. Particular emphasis is placed on the description of the broadband dye laser.

A characteristic feature of broadband laser radiation is the random nature in the temporal domain. The intensity changes randomly in time during the laser pulse. Thus the broadband laser radiation most resembles an interval of spontaneous noise where the interval is defined by the pulse envelope. The ouput pulses of a dye laser pumped by a nanosecond pulses, have a duration of the order of 10 ns. The spontaneous noise appears in the temporal domain as a chaotic sequence of intensity spikes and deep 'valleys', almost reaching zero.

The main assumptions of the model are as follows :

- The nonlinear interaction of the radiation with the resonator elements is negligibly small. This ensures the independence and random nature of the amplitude and phases of the longitudinal modes.
- The only effect of the saturation of the amplifying medium is to stabilise the total pulse energy.
- Only the lowest transverse mode is present.
- Many longitudinal modes are present.

The model presented here is classical in nature as the only point at which a quantum description could be required is in the dynamics of spontaneous radiation. This is treated through the introduction of spontaneous noise.

A broadband laser pulse is generated through the amplification of initial spontaneous noise. The statistics of the initial spontaneous noise is known to be Gaussian [24]. As amplification and frequency filtration are linear operations which do not change the Gaussian character of the radiation, one might expect the broadband laser radiation to be Gaussian in character. However, this is only true if the saturation of the active medium is disregarded. This saturation is a nonlinear process which acts to distort the Gaussian character of the radiation.

The nonlinear nature of the energy stabilisation is easily recognised in the limitations this imposes on the intensity range of the radiation. For pure Gaussian noise there is no such limitation.

Masalov [24] has shown that the statistics of broadband laser radiation depends on the number of generated longitudinal modes. For a small number N of longitudinal modes the difference from the Gaussian statistics is large, while for large N the difference becomes very small. For the broadband dye laser used for CARS work, the number of longitudinal modes generated is very large (typically $\sim 10^4$) and the longitudinal mode structure is not pronounced. Therefore the broadband dye laser radiation is expected to be Gaussian in character.

For broadband radiation obeying Gaussian statistics it is convenient to write the electric field in the form [24]

$$E(t) = \sqrt{p(t)}\varepsilon(t)e^{2\pi i\nu_0 t} \tag{2}$$

where $p(t)$ represents the pulse envelope, ν_0 is the central radiation frequency, and $\varepsilon(t)$ is a complex amplitude of Gaussian noise representing the amplitude of the amplified spontaneous noise. $\varepsilon(t)$ is suitably frequency filtered so that the spectrum of $\varepsilon(t)$ coincides with the spectrum of the output radiation. By definition, the Gaussian nature of the statistics of $\varepsilon(t)$ means that its distribution is normal. It is not necessary to introduce coordinates describing the beam cross-section into Equation 2 as one of the assumptions of the model is that only the lowest transverse mode is being considered.

The intensity of the radiation is given by

$$\begin{aligned} I(t) &= E^*(t)E(t) \\ &= p(t)\varepsilon^*(t)\varepsilon(t) \end{aligned} \tag{3}$$

This is just the intensity of the Gaussian noise modulated by the pulse envelope.

Note that the effects of nonlinear interaction such as nonlinear absorbtion, self-phase modulation, etc. ,with the resonator elements have been ignored. The effects of nonlinear interactions depend on the beam intensity and on the type of interaction. Thus it is difficult to formulate a model of laser radiation which allows a description of the radiation with nonlinear effects. For lasers in which nonlinear interactions cannot be ignored, the properties of Gaussian statistics cannot be applied to the complex amplitude $\varepsilon(t)$. However, Masalov [24] has shown that, for nonlinear interactions, the number of modes necessary to ensure the Gaussian character of laser radiation increases with the interaction nonlinearity, and for a very large number of modes (such as the 10^4 dye laser modes), the radiation statistics in K-photon processes is expected to be equivalent to radiation with Gaussian statistics for a large range of K.

Measurements of 5-photon sodium atom ionization using a broadband neodymium-glass laser ($\sim 10^4$ longitudinal modes) have shown within experimental error that the radiation of this laser is equivalent to radiation with Gaussian statistics in nonlinear interactions at least for $K \leq 5$ [25]. Extension of this result to the broadband dye laser and to higher order nonlinear processes requires experimental verification.

The intensity distribution for radiation which can be described using Gaussian statistics is well known and is given by

$$P(I) = \frac{1}{\langle I \rangle} exp(-\frac{I}{\langle I \rangle}) \tag{4}$$

where $\langle I \rangle$ is the mean radiation intensity which is time dependent for pulsed lasers. Note that no limitations are placed on the spectral shape of the pulse by the use of Gaussian statistics. The spectrum may assume any shape. For an exponential distribution, the most probable value of the intensity is zero, but the distribution admits arbitrarily large values for I. This property distinguishes Gaussian noise from real radiation where clearly there are always energy constraints which limit the maximum permissible intensity. However, as already mentioned, lasers operating within the constraints of the model and with a large number of longitudinal modes should obey Gaussian statistics.

The analysis thus far has been limited to temporal fluctuations of laser radiation. A general analysis of spectral fluctuations of broadband laser radiation

is absent from the literature. The reason for this is linked to the effects of amplification saturation on different modes. For modes with a low average energy which lie in the spectrum wings, the effects of amplification saturation are less pronounced than for those with a higher mean energy whose frequencies lie near the spectrum maximum. The mode energy distribution for the modes in the wings differs little from an exponential distribution while that of the central frequency modes differs most. Therefore the formulation of an energy distribution which is valid for all spectral modes is a non-trivial problem.

The main characteristics of the spectral structure of broadband laser radiation can be obtained from its temporal structure. The amplitude spectrum $s(\nu)$ of a given pulse can be obtained through Fourier transformation from the time domain field amplitude $E(t)$ in the usual manner :

$$\begin{aligned} s(\nu) &= \int E(t)e^{-2\pi i\nu t}dt \\ E(t) &= \int s(\nu)e^{2\pi i\nu t}dt \end{aligned} \tag{5}$$

For our model, the time domain field amplitude $E(t)$ is an interval of Gaussian noise. Fourier transformation is a linear process and thus the Gaussian character of the statistics is preserved. Therefore $s(\nu)$ also has the properties of Gaussian noise. Masalov [24] shows that the interval which characterizes the frequency scale of the random structure in the spectrum is given by the inverse pulse duration $1/T_p$.

The quantity which is measured by the detector pixels is the energy spectrum $S(\nu)$ where

$$\begin{aligned} S(\nu) &= \mid s(\nu) \mid^2 \\ &= \int\int E^*(t)E(t+\tau)e^{2\pi i\nu\tau}dtd\tau \end{aligned} \tag{6}$$

The energy distribution is exponential due to the Gaussian nature of the amplitude spectrum and is given by

$$P(S(\nu)) = \frac{1}{\langle S(\nu)\rangle}exp(-\frac{S(\nu)}{\langle S(\nu)\rangle}) \tag{7}$$

where $\langle S(\nu) \rangle$ is the average radiation spectrum.

The ideal device for observing pulse spectra should have a spectral resolution $\Delta\nu$ which does not exceed $1/T_p$. For such a device, the observed spectra should have a random structure with deep drop-offs, almost reaching zero, and with a frequency scale $\sim 1/T_p$. Unfortunately, for a pulsed dye laser with a pulse length of the order of 10 ns the resolution required is very high $\sim 0.003\ cm^{-1}$. The highest possible resolution of the OMA used for the measurements corresponded to one detector pixel, giving a resolution of $\sim 0.15\ cm^{-1}$. This is well below the ideal resolution. Another effect resulting in a further loss of resolution, not accounted for thus far, is the cross-talk between adjacent detector pixels ($\sim 3 - 5$ pixels for the OMA used).

The effect of using a spectral device with a lower resolution is to cause a smoothing of the random structure of the spectrum. In this case the frequency scale of the structure is of the order of the instrument resolution $\Delta\nu$ and the relative depth of the structure is $\sim \sqrt{\Delta\nu T_p}$.

The model presented here has only taken account of the statistical properties of broadband pulse spectra. Random structure in spectra can also be related to the frequency selective properties of resonator elements and structure of the optical transition of the active medium. These effects have not been addressed. Further, in the interaction with matter, it is only in the simplest cases that the spatial structure of the lowest transverse mode can be neglected. In addition, this analysis takes no account of broadband laser radiation where more than one transverse mode is present. Therefore, the model is only a first approximation to broadband laser radiation and further work in this field is warranted.

3 Experimental Setup

The experimental setup used was as given in Figure 2.

3.1 Nd:YAG Laser

A pulsed Nd:YAG laser, operating in a single longitudinal mode, was used for the measurements. The beam is initiated by flashlamp excitation of the Nd:YAG crystal in the oscillator and an infrared pulse with a wavelength of 1064 nm is produced. The pulse length is of the order of 13 ns with a linewidth less than 0.001 cm^{-1} [12]. The oscillator is Q-switched using a saturable absorber dye.

The laser pulse from the oscillator is allowed to expand by diffraction along a 6 m path and then amplified using two flashlamp-driven amplifiers in series. The beam expansion is necessary in order to fill the amplifier rods. The frequency of the pulse is then doubled by propagation through a KDP crystal. The wavelength of the pulse after frequency doubling is 532.0 nm and the beam appears in the green region of the visible spectrum. A portion of the beam (10 %) is then split off to pump the dye laser oscillator and another portion (25 %) is split off to pump the dye laser amplifier. The remainder of the green beam propagates along an optical delay path of the order of 1.3 m before combining with the dye laser beam. The delay path is necessary as the dye laser takes time to reach threshhold and the two beams must be coincident for CARS work.

3.2 Broadband Dye Laser

The dye laser consists of two components: an oscillator and an amplifier. The oscillator cavity length is 60 cm. Dye is pumped through a dye cell of active length $\sim$ 1 cm in each component with separate dye circuits for the oscillator and amplifier. Thus different dye concentrations can be used in the oscillator and amplifier. Each dye circuit contains approx. 500 ml of dye solution. The two dye cells are transversely pumped by split-off portions of the frequency-doubled Nd:YAG beam.

The dye laser is tuned by varying the dye concentrations in the oscillator and amplifier. The wavelength of the broadband laser peak is required at 606.7 nm for CARS using this system. Thus the dye beam appears in the

orange region of the visible spectrum. The bandwidth of the dye laser beam was typically of the order of 3 nm.

3.3 CARS Cell and Spectrometer

For colinear CARS measurements, the coincident pump (green frequency-doubled Nd:YAG beam) and Stokes beams (orange dye laser beam) are brought to a focus in the gas cell of interest. The emerging coincident beams, which includes a CARS beam (cf. Section 2.1), are recollimated using another lens and pass through a dichroic filter which allows transmission of the CARS beam only. The pump and Stokes beams are stopped in a beam trap. The CARS beam is focussed onto a slit at the entrance to the spectrometer and then diverges and falls onto a holographic grating. The grating focusses the beam to a line focus using the astigmatism built into the grating and the beam then passes through a focussing telescope and is directed onto the 1024 detector pixels of the PARC EG&G 1421 Optical Multichannel Analyser (OMA). A PARC 1461 Detector Interface is used for the detector control and the digital recording of the signal.

The digitally recorded CARS signal is then corrected for detector background noise, by subtracting a scan taken in between the laser firing intervals. Contributions to the background noise originate from detector dark current or noise present in the absence of a signal and from scattered light present in the laboratory.

Measurements of the dye laser beam on its own were taken by blocking off the Nd:YAG beam immediately after the pumping of the dye laser. For these measurements. the gas cell and focussing lenses for CARS generation were removed and the dye laser was directed into the spectrometer.

The spectrometer dispersions were as follows :

- Dye laser beam at 606.7 nm : dispersion 5.629×10^{-3} $nm/pixel$
- CARS signal at 473.7 nm : dispersion 6.411×10^{-3} $nm/pixel$
- Frequency-doubled Nd:YAG at 532.0 nm : dispersion 6.101×10^{-3} $nm/pixel$

The SOPRA Users Manual [26] gives more detail on the laser system.

Table 1: Dye names

abbreviation	*cross name*	*Lambda Physik name*	*Code*
Rh610	Rhodamin 610	Rhodamin B	LC 6100
Rh640	Rhodamin 640	Rhodamin 101	LC 6400
SfRh101	Sulforhodamin 101	Sulforhodamin 101	LC 6600

4 Dye Laser Method

As mentioned in the introduction, preliminary dye laser spectral measurements in May 1991 and June 1992 had led to some inconclusive results and a much more thorough and systematic investigation of dye mixtures and methods of tuning the dye laser was necessary. For the nitrogen thermometry CARS work being performed, the dye laser was required to peak at 607 nm. Combinations of three dyes, producing an output at the correct wavelength, have been investigated. The three dyes were purchased from Lambda Physik and are referred to in this thesis by the abbreviations. The full names and codes of the dyes are as given in Table 1.

4.1 Concentrations

The transversely-pumped dye laser consists of two separate dye circuits : an oscillator- and an amplifier circuit. Preliminary measurements in May 1991 and June 1992 seemed to indicate that the method of tuning the dye amplifier may be a significant factor contributing to spectral fluctuations. Two methods were employed to optimize the concentrations for the dye mixtures, differing in the concentrations used in the amplifier. These were as follows :

- **Method of $\frac{1}{3}$ concentration :** Rh610 is added to the dye oscillator to maximise the output intensity. The second dye (Rh640 or SfRh101) is then added to tune the oscillator to the required wavelength. One third of the oscillator concentrations is then used in the amplifier. Where this method has been used, it is denoted by ($\frac{1}{3}$ conc).
- **Method of tuning amplifier :** The oscillator is tuned as for the method above. One third of the Rh610 is then added to the amplifier and then the second dye (Rh610 or SfRh101) is added to the amplifier so that the amplifier is tuned to the correct wavelength on its own. This results in there being a greater concentration of the second dye in

the amplifier than in the oscillator. Where this method has been used, it is denoted by (tuned).

The dyes, which were initially in powder form, were disolved in ethanol. An increase in dye concentration results in a shift toward longer wavelengths. A theoretical explanation for this is given by Schäfer [27].

Another factor which must be considered in the choice of dyes and concentrations is that the lower the dye concentration, the less the output power. This is true below the optimum concentration for the dye where the output power is a maximum. It is for this reason that SfRh101 on its own is not satisfactory for CARS work where the dye laser is required to peak at 607 *nm* despite being the least noisy of the dyes. The maximum power output using the SfRh101 dye occurs at longer wavelengths and the dilution required to shift the laser emission to shorter wavelengths is at the expense of beam power.

As a number of dye combinations and concentrations have been investigated and are presented in this thesis, there is the risk of confusion between them. In order to avoid this, letter codes have been introduced. These are given below :

- **A**: Rh640 in the oscillator only.
- **B**: SfRh101 in the oscillator only.
- **C**: Rh610 in the oscillator only.
- **D**: Rh610/Rh640 mixture in the oscillator only.
- **E**: Rh610/Rh640 mixture in the oscillator. Rh610/Rh640 mixture in the amplifier ($\frac{1}{3}$ conc).
- **F**: Rh610/Rh640 mixture in the oscillator. Rh610/Rh640 mixture in the amplifier (tuned).
- **G**: Rh610/SfRh101 mixture in the oscillator only.
- **H**: Rh610/SfRh101 mixture in the oscillator. Rh610/SfRh101 mixture in the amplifier ($\frac{1}{3}$ conc).
- **I**: Rh610/SfRh101 mixture in the oscillator. Rh610/SfRh101 mixture in the amplifier (tuned).

Table 2: Dye concentrations used.

letter code	*dye*	*oscillator*	*amplifier*
A	Rh640	66mg/500ml	
B	SfRh101	42mg/500ml	
C	Rh610	96mg/500ml	
D	Rh610	95mg/500ml	
	Rh640	8.6mg/500ml	
E	Rh610	95mg/500ml	31mg/500ml
	Rh640	8.6mg/500ml	2.8mg/500ml
F	Rh610	95mg/500ml	31mg/500ml
	Rh640	8.6mg/500ml	14mg/500ml
G	Rh610	91mg/500ml	
	SfRh101	18mg/500ml	
H	Rh610	91mg/500ml	30mg/500ml
	SfRh101	18mg/500ml	6.0mg/500ml
I	Rh610	91mg/500ml	30mg/500ml
	SfRh101	18mg/500ml	31mg/500ml

Table 3: Beam power readings

letter code	*source*	*energy (mJ)/pulse*
	Nd:YAG (532nm)	140
E	Rh610/Rh640 ($\frac{1}{3}$ conc)	0.6
F	Rh610/Rh640 (tuned)	0.6
H	Rh610/SfRh101 ($\frac{1}{3}$ conc)	0.9
I	Rh610/SfRh101 (tuned)	0.6

In addition, non-resonant CARS spectra, generated in a reference cell containing Argon at a pressure of 40 Bar, have been observed using **E**, **F**, **H**, and **I**. The letter codes assigned to these are **E-CARS**, **F-CARS**, **H-CARS**, and **I-CARS**, respectively.

The concentrations used are given in Table 2.

4.2 Beam power readings

The beam power readings were as given in Table 3. Power readings were taken with the laser operating at 5 Hz using a Scientech 380101 Calorimeter. The uncertainty in the power readings is $\pm 0.2\ mJ$.

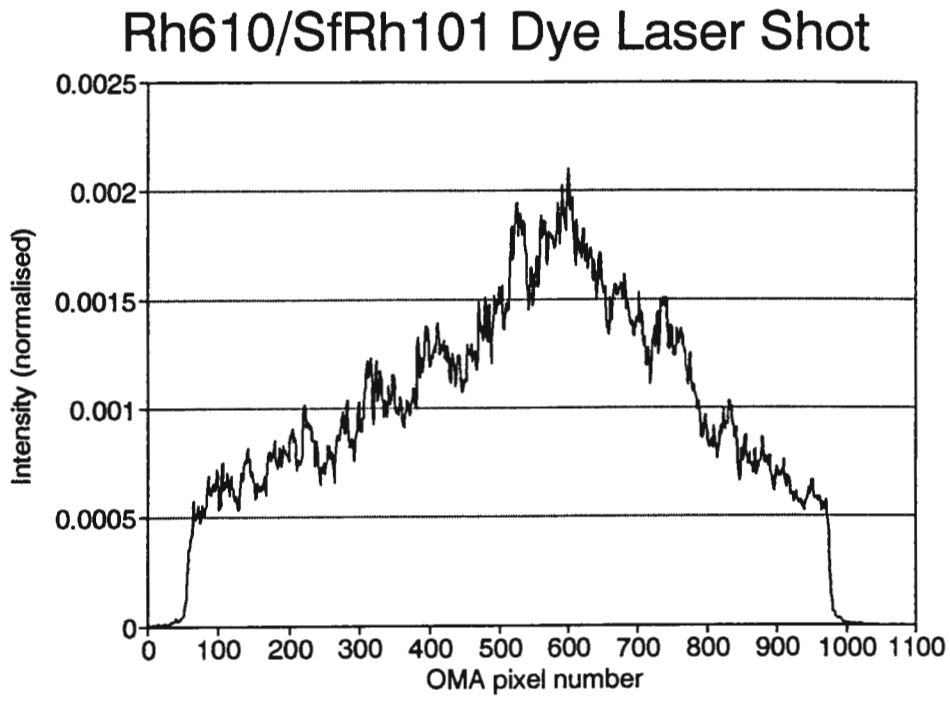

Figure 3: Typical dye spectrum for Rh610/SfRh101 ($\frac{1}{3}$ conc.)

Runs of 50 shots (usually 6 runs) at 5 Hz were taken for each dye combination. The spectra were recorded using all 1024 pixels of the OMA (cf. Section 3). In addition, as already mentioned, non-resonant CARS spectra were obtained from a CARS reference cell containing Argon at a pressure of 40 bar. A typical dye laser spectrum (single shot) from run **H** is shown in Figure 3 and a typical CARS spectrum (single shot) from run **H-CARS** is shown in Figure 4. Note how the non-resonant CARS spectrum takes on the shape of the dye laser spectrum and is slightly less jagged, indicating that the CARS spectrum is less spectrally noisy.

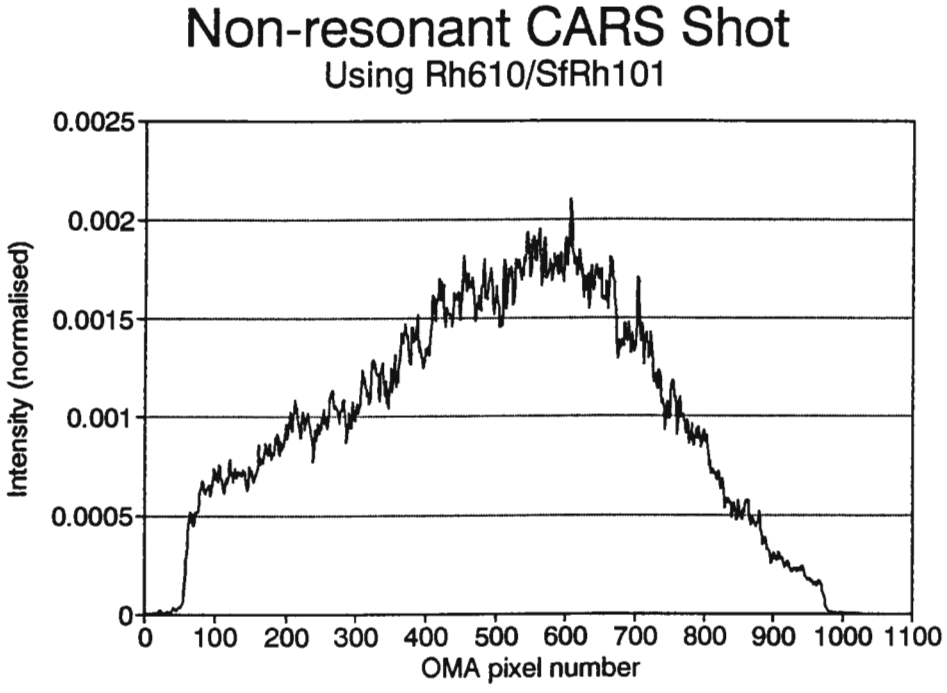

Figure 4: Typical CARS spectrum for Rh610/SfRh101 ($\frac{1}{3}$ conc.)

5 Methods of Analysis

The data analysis of the spectra obtained involves the problem of finding a suitable measure of spectral fluctuations. This did not turn out to be a trivial problem and various methods were attempted as outlined below:

5.1 Sum of squares of deviations

The first method used is intuitive and was intended as a preliminary method in order to get some feel for the data. This method was applied to the May 1991 measurements for which runs of 30 shots were taken (runs of 50 shots were taken during the most recent measurements). During these measurements, a preliminary comparison was made between the Rh610/Rh640 mixture and SfRh101 on its own.

For each run of thirty shots, each shot was normalised to constant energy such that the integral of the counts taken over all 1024 pixels of the OMA was equal to 10^4. Note that 10^4 is entirely arbitrary and was used as a basis for comparison between the dyes merely because it gave conveniently sized numbers with which to work. Normalisation was used since, in CARS work, the spectral shape is of greater importance than shot-to-shot energy fluctuations.

Expressed mathematically, the spectra were normalised such that :

$$\sum_{i=1}^{1024} \mathrm{I}_i^{(k)} = 10^4 \tag{8}$$

where $\mathrm{I}_i^{(k)}$ represents the number of counts recorded in pixel i of the normalised shot k .

An average normalised spectrum $(\mathrm{Av})_i$ was then calculated for the file (usually 30 shots, but dud shots had to be removed for some runs) such that :

$$(\mathrm{Av})_i = \frac{1}{\mathrm{N}} \sum_{k=1}^{\mathrm{N}} \mathrm{I}_i^{(k)} \tag{9}$$

where N is the number of shots for the file.

The sum of the squares of the deviations $\mathrm{S}^{(k)}$ of each normalised spectrum k

from the average normalised spectrum was then calculated such that :

$$S^{(k)} = \sum_{i=1}^{1024} [\ (Av)_i - I_i^{(k)}\ ]^2 \qquad (10)$$

An average $S^{(k)}$ was found for each file as well as the standard deviation of the mean. Using this method, a low value of $S^{(k)}$ indicates few spectral fluctuations while a high value indicates poor spectral reproducibility.

The mean value of $S^{(k)}$ for SfRh101 on its own was 996, while that for the Rh610/Rh640 mixture was 8675. These results showed clearly that SfRh101 was considerably less spectrally noisy than the Rh610/Rh640 mixture. A few runs of the Rh610 on its own were also taken and a value of 6359 for $S^{(k)}$ was calculated. Not too much confidence should be placed on this value as, unlike for the other measurements, only alternate detector pixels (512 of them) were in operation at the time and the effects of detector cross-talk would not be the same as for the other measurements. However, this value showed that a significant portion of the noise was a result of some intrinsic property of the Rh610 dye.

During these May 1991 measurements, non-resonant CARS was also generated in a reference cell containing Argon and values of 7423 and 1120 for $S^{(k)}$ were calculated from the CARS spectra using the Rh610/Rh640 mixture and the SfRh101 dye, respectively. Thus it was clear that the spectral noise in the non-resonant CARS signal followed the noise in the dye laser.

This method of quantifying spectral fluctuations produces meaningful results and could be used for noise comparison, but it is crude in its approach and not mathematically elegant. For example, the choice of 10^4 counts as the normalisation energy is entirely arbitrary. A more refined approach is in order.

5.2 χ^2 reproducibility test

χ^2 tests are used to compare observed with expected frequencies and so this seemed like an obvious test to apply to the dye laser spectra. Two procedures were attempted which differed in their normalisation of the spectra :

5.2.1 Method A

Method A involved the same normalisation procedure as for Section 5.1 ie. the spectra were normalised such that the total number of counts for each spectrum was 10^4 (see Equation 8) . An average spectrum $(\mathrm{Av})_i$ was once again found for the file (usually 30 shots) from the normalised spectra. The χ^2 test statistic was calculated for each shot k in the file where :

$$\chi^2_{(k)} \equiv \sum_i \frac{(\mathrm{I}_i^{(k)} - (\mathrm{Av})_i)^2}{(\mathrm{Av})_i} \tag{11}$$

where:

- $\mathrm{I}_i^{(k)}$ - no. of counts recorded in pixel i of the normalised spectrum k.
- $(\mathrm{Av})_i$ - no. of counts in pixel i for the average spectrum

For a χ^2 test with large degrees of freedom (> 30), the test statistic

$$\mathrm{N} \equiv \sqrt{2\chi^2} - \sqrt{2\nu - 1} \tag{12}$$

should be very nearly normally distributed with mean zero and standard deviation one. This was also calculated. The degrees of freedom ν were taken as :

$$\nu = (\ \textit{pixels processed}\ ) - (\ \textit{parameters estimated from data}\ ) - 1 \tag{13}$$

The number of parameters estimated from the data was not straightforward. A logical step was to take this quantity as unity as only the mean was estimated. However, as the mean had to be found for each pixel, it seemed doubtful that taking a value of unity was correct. Note that if one considers the mean calculated for each pixel as a separate quantity, the number of quantities estimated from the data would be equal to the number of pixels

processed which would give a negative ν-value. This does not make sense. Therefore it was decided to take ν as unity.

The results yielded values for N which were too far from zero to be instructive. Thus the χ^2 test broke down when applying it to the data. Tests such as the χ^2 test rely on the statistical independence of the data set. One way in which the data set may lose its statistical independence is through detector cross-talk. This is a well known effect whereby there exists energy splashover between adjacent pixels of the OMA. The energy splashover is typically of the order of three pixels. Thus by sampling every 20th pixel, for instance, one should eliminate detector cross-talk effects from the data and obtain a statistically independent data set. This procedure was attempted, but the χ^2 test still broke down though the values of N did approach zero slowly when fewer pixels were sampled.

The only plausible explanation for the failure of the χ^2 test seemed to be that there existed long-range spectral correlations between modes of the dye laser. This was in contrast to many of the views expressed in the literature (cf. Section 1).

Note that the observed and expected values must occur with a frequency of > 5 for a χ^2 test to be used and so only the mid 1000 pixels were sampled (instead of all 1024) although sampling all the pixels made very little difference.

5.2.2 Method B

The normalisation procedure of Method B differs from that of Method A. Let $I_i^{(k)}$ be the number of counts recorded by pixel i for shot k. A standardised average spectrum $(\mathrm{Ref})_i$ was found such that :

$$(\mathrm{Ref})_i \equiv \frac{\sum_{k=1}^{no.shots} I_i^{(k)}}{\sum_{k=1}^{shots} \sum_{i=1}^{pixels} I_i^{(k)}} \tag{14}$$

so that $\sum_i (\mathrm{Ref})_i = 1$. Then for spectrum k :

$$\chi^2_{(k)} \equiv \sum_i^{pixels} \frac{(I_i^{(k)} - \mathcal{N}_{(k)}(\mathrm{Ref})_i)^2}{\mathcal{N}_{(k)}(\mathrm{Ref})_i} \tag{15}$$

where $\mathcal{N}_{(k)} = \sum_{i=1}^{pixels} I_i^{(k)}$ (ie. the total number of counts in 1024 pixels).

In this way the expected frequency for pixel i (given by $\mathcal{N}_{(k)}(\mathrm{Ref})_i$) were scaled according to the energy of the particular shot. Once again the pixels

at the edges of the detector were not used due to the same reasons as in Method A, however, these were included in the calculation for $(\text{Ref})_i$ and $\mathcal{N}_{(k)}$.

The results showed the same trends as Method A, but with larger values for N since the shots were not scaled down to 10^4 counts.

Both these methods were instructive, but did not yield any useful results. The failure of these tests pointed to the existence of significant correlations between modes of the dye laser. This required further investigation and a new approach was called for.

5.3 Cross correlation reproducibility test

The next method attempted of analysing spectral fluctuations in the May 1991 data was to calculate the correlation coefficient for a particular shot and the average of the rest of the shots in the file. No normalisation was used. The correlation coefficient $r^{(k)}$ corresponding to shot k is given by :

$$r^{(k)} \equiv \frac{\sum_i (I_i^{(k)} - \bar{I}^{(k)})(I_i^{(ave)} - \bar{I}^{(ave)})}{[\sum_i (I_i^{(k)} - \bar{I})^2 \sum_i (I_i^{(ave)} - \bar{I}^{(ave)})^2]^{\frac{1}{2}}} \tag{16}$$

where :

- $I_i^{(k)}$ is the no. of counts recorded by pixel i for shot k.
- $\mathcal{N}$ = total no. of pixels
- $\mathcal{S}$ = total no. of shots
- $\bar{I}^{(k)} = \frac{1}{\mathcal{N}} \sum_{i=1}^{\mathcal{N}} I_i^{(k)}$
- $I_i^{(ave)} = \frac{1}{\mathcal{S}-1} [\sum_{j=1}^{k-1} I_i^{(j)} + \sum_{j=k+1}^{\mathcal{S}} I_i^{(j)}]$
- $\bar{I}^{(ave)} = \frac{1}{\mathcal{N}} \sum_{i=1}^{\mathcal{N}} I_i^{(ave)}$

Thus a value for $r^{(k)}$ for each shot k in a file of usually 30 shots (sometimes less due to dud shots) was found.

5.3.1 $\mathcal{Z}$ Parameter

In order to obtain information about the distribution of $r^{(k)}$ it was necessary to introduce the $\mathcal{Z}$ parameter. The $\mathcal{Z}$ parameter was calculated from the correlation coefficient $r^{(k)}$ for each shot k using the equation :

$$\mathcal{Z}^{(k)} = \frac{1}{2} \ln \frac{1 + r^{(k)}}{1 - r^{(k)}} \tag{17}$$

According to statistical methods. $\mathcal{Z}^{(k)}$ should be normally distributed about the mean $\overline{\mathcal{Z}} = \ln \frac{1+\rho}{1-\rho}$ where ρ is the "population" correlation coefficient.

Also, $\mathcal{Z}$ should have a variance $\sigma_z = \frac{1}{\sqrt{N-3}}$. It is unclear exactly what this N refers to in our case where correlations between pixels appear to exist.

5.3.2 Dimensionless Moments About Mean For $\mathcal{Z}$

Dimensionless moments about the mean for $\mathcal{Z}$ were calculated for each file as follows:

The r_{th} moment about the mean m_r is given by :

$$m_r \equiv \frac{1}{\mathcal{S}} \sum_{k=1}^{\mathcal{S}} (\mathcal{Z}^{(k)} - \overline{\mathcal{Z}})^r \tag{18}$$

Recall from Equation 16 that $\mathcal{S}$ refers to the total number of shots in the file. The dimensionless moment a_r is given by :

$$a_r \equiv \frac{m_r}{(\sqrt{m_2})^r} \tag{19}$$

Note that the standard deviation is given by $s \equiv \sqrt{m_2}$. If $\mathcal{Z}$ were normally distributed about $\overline{\mathcal{Z}}$, we would have $a_3 = 0$ and $a_4 = 3$. The values for a_3 and a_4 were calculated for each file using the May 1991 data. The results obtained indicated that $\mathcal{Z}$ was not nearly normally distributed, thus casting doubt over the applicability of this method in analysing the data set. An unknown quantity was the distorting effect mode correlations might have on the statistical distributions.

The reproducibility comparison using this method shows that the spectra obtained using the SfRh101 dye are more reproducible than those obtained using the Rh610/640 mixture. An average value of $r^{(k)}$ was found for each file and the mean value for the SfRh101 files was 0.973. The corresponding value for the Rh610/Rh640 mixture was 0.845. Thus, the same conclusion was reached using this method as the Sum of the Squares of the Deviations Method discussed in Section 5.1. The question remained as to which method, if any, was the most statistically sound so that it could be used as the standard test for reproducibility of spectra.

5.4 Auto-correlation Analysis of Spectra

The results of previous sections have shown that neighbouring pixels of the OMA are not independent. This is witnessed by the failure of the standard statistical tests to produce meaningful results. Standard tests such as the χ^2 test rely on the independence of the members of the data set on which the test is being applied. It has become clear that this is not the case for the detector pixels.

The detector array used for the measurements is known to have an energy splash-over extending over approximately 3 pixels. Therefore, by sampling every twentieth or fiftieth pixel an independent data set of random variables should be obtained. The results of Section 5.2 have shown that this is not the case. Therefore, the assumption of independent modes of the dye laser would appear to be false. In this section, an investigation is made into the correlation between the modes of the dye laser. The correlation between neighbouring groups of modes is investigated using auto-correlation functions. Two auto-correlation functions have been investigated (labeled A and B) and differing in definition. Use of auto-correlation functions applied in this way in the analysis of mode correlations does not appear in the literature.

5.4.1 Auto-correlation Function Method A

The first auto-correlation function investigated is as defined below. All 1024 detector pixels were processed and no normalisation of the shots was used as this has no effect on the results using this method. The auto-correlation function corresponding to a difference of i between correlated pixels is given by :

$$\Phi(i) \equiv \frac{\sum_{j=1}^{1024-i} Y_j Y_{j+i}}{(\sum_{j=1}^{1024-i} Y_j^2)^{\frac{1}{2}} (\sum_{j=1}^{1024-i} Y_{j+i}^2)^{\frac{1}{2}}} \tag{20}$$

where :

- $Y_j = I_j - \bar{I}$
- I_j is no. of counts recorded by pixel j
- $\bar{I} = \frac{1}{1024} \sum_{j=1}^{1024} I_j$

Plots were made of $\Phi(i)$ vs i. For independent dye laser modes, one would expect the autocorrelation function to drop to and hover around zero after a pixel gap of the order of a few tens of pixels. The drop to zero would not happen after only one or two pixels as there is some cross-talk between adjacent pixels of the OMA. Thus for independent modes, the auto-correlation function would be a reflection of detector characteristics.

Another factor which has to be taken into consideration is that spectral peaks can have surprisingly long tails. This effect could be responsible for a slower drop-off rate of the correlation function.

The plots did indeed show slower drop-off rates with the auto-correlation coefficient dropping to zero only after a gap of 200 - 300 between correlated pixels. This was, however, much slower than expected even considering the 'long tails'. This was indicative of the presence of mode correlations and is discussed further in Section 5.4.2.

Another surprising feature was that after reaching zero, the auto-correlation functions did not hover around zero but dropped well below it, reaching a trough after a pixel gap between correlated pixels of between 500 - 700 pixels. Thereafter, the functions rose above zero again for some shots. From these observations, it became apparent that the definition of the auto-correlation function used (see Equation 20) and in particular the definition of the $\bar{I}$ value was responsible for the strange shapes of the auto-correlation curves. A new auto-correlation method was required which reduced the effect of the overall spectral shape.

5.4.2 Auto-correlation Function Method B

Results for the autocorrelation calculations using the first method seemed to be very dependent on the large scale shape of the spectra. The subtraction of the constant average value $\bar{I}$ in the autocorrelation function calculations appeared to be responsible for the strange shapes being obtained. Method B reduces this dependence by calculating the autocorrelation function for the noise spectra.

These noise spectra are obtained by first normalising the shots in the run to constant integrated energy, finding the average normalised spectrum for the run and then subtracting this average normalised spectrum from each normalised spectrum in the run. The auto-correlation calculations are performed on each noise spectrum and the from these, the average auto-correlation function for the file is calculated.

A number of pixels (100) was dicarded from each end of the OMA for these calculations in order to remove instrument effects at the edge of the array. It was found that this made negligible difference to the auto-correlation functions.

Mathematically :

Let $I_i^{(k)}$ be the counts recorded by pixel i for shot k and let $\mathcal{S}$ be the total no. of shots in the run. Normalise each pixel according to :

$$N_i^{(k)} \equiv \frac{I_i^{(k)}}{\sum_{i=1}^{1024} I_i^{(k)}} \tag{21}$$

Find the average normalised spectrum :

$$\overline{N_i} \equiv \frac{\sum_{k=1}^{\mathcal{S}} N_i^{(k)}}{\mathcal{S}} \tag{22}$$

Calculate the auto-correlation function corresponding to a difference of j between correlated pixels :

$$\Phi(j) \equiv \frac{\sum_{i=1}^{pix-j} Y_i^{(k)} Y_{i+j}^{(k)}}{(\sum_{i=1}^{pix-j} (Y_i^{(k)})^2)^{\frac{1}{2}} (\sum_{i=1}^{pix-j} (Y_{i+j}^{(k)})^2)^{\frac{1}{2}}} \tag{23}$$

where : $Y_i^{(k)} = N_i^{(k)} - \overline{N_i}$.

Plots were made of $\Phi(j)$ vs j. The term 'pixel gap' in the plots refers to the difference in correlated pixels. Figure 5 shows a plot of $\Phi(j)$ for j in the range of 0 to 30 pixels for **B** and **C** which correspond to SfRh101 and Rh610 in the oscillator, respectively (cf. Section 4.1 for explanation of letter codes). Both plots show a sharp drop-off from zero to three pixels, a slight rounding out from about pixel 3 to pixel 15 and a more gradual decrease from about pixel 15 onwards. These first of these three regions should correspond to the instrument function effect of cross-talk, the second should correspond to the "tail" region of the peaks and the third should correspond to correlations between groups of modes.

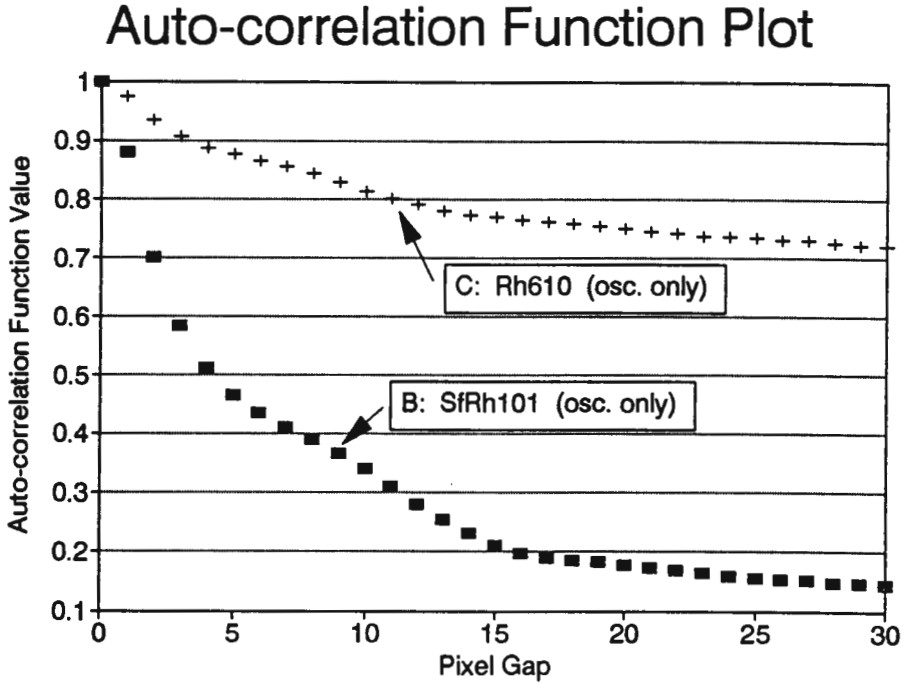

Figure 5: Dye spectra auto-correlations for SfRh101 and Rh610 (oscillator only)

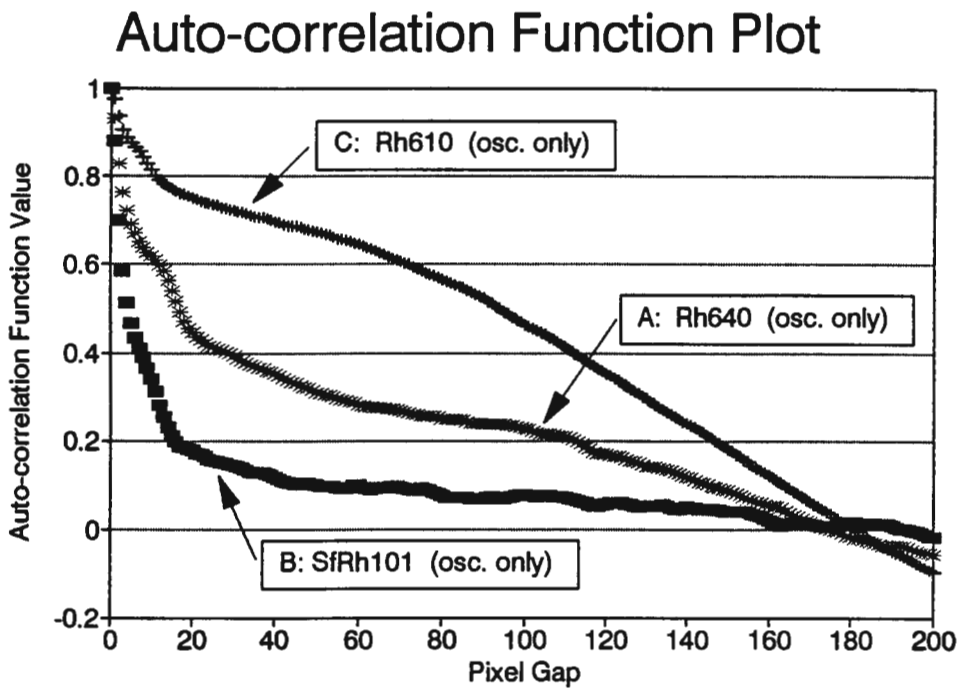

Figure 6: Dye spectra auto-correlations for Rh640, SfRh101, and Rh610 (oscillator only)

Figure 6 shows $\Phi(j)$ vs j for **A**, **B**, and **C** plotted for a j in the range of 0 to 200 pixels. The most striking feature of the plot is the difference in the degree of correlation between groups of modes for the three dyes. The Rh610 clearly shows very significant correlations between groups of modes while the SfRh101 shows little correlation. The plot for Rh640 lies in between the other two plots. Thus it has been shown not only that correlations *do* exist between modes of the dye laser, but also that the degree of correlation can vary between dyes.

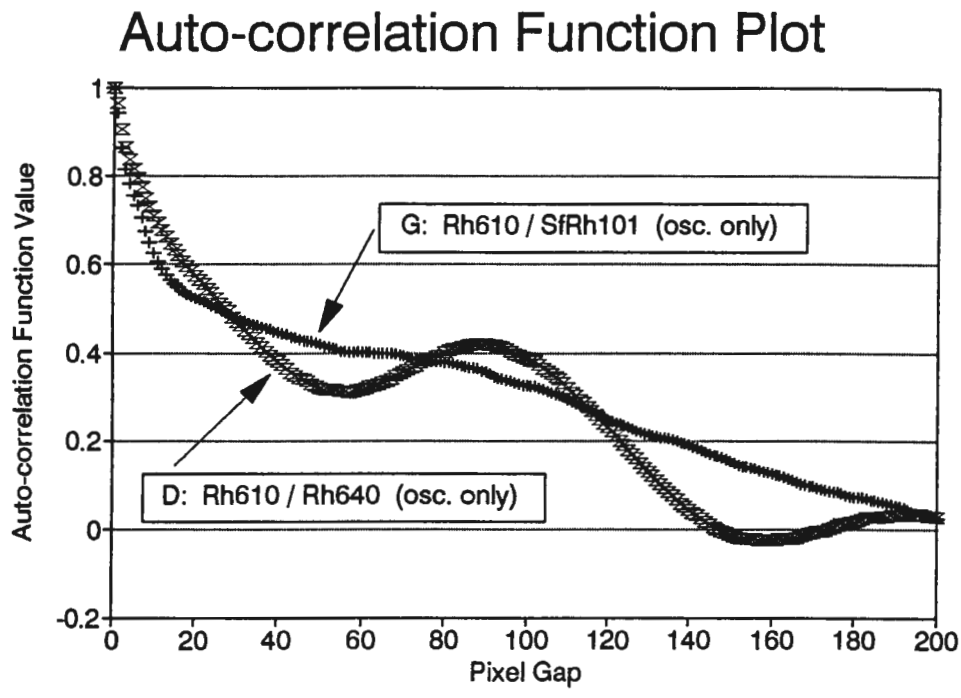

Figure 7: Rh610/Rh640 and Rh610/SfRh101 dye spectra auto-correlations (oscillator only)

As mentioned in Section 4.2, six runs of 50 shots were taken for each dye combination. The auto-correlation plots shown in this section are the average auto-correlation functions from one of the six runs. It was not crucial as to which run was chosen as it was observed that, on the whole, the six auto-correlation plots for any particular dye combination were very tightly grouped. Thus the auto-correlation plots show inherent structure in the spectra which is characteristic of the dye being used.

Figure 7 shows the auto-correlation functions for **D** and **G** which are runs taken using the dye oscillator only for the Rh610/Rh640 mixture and the Rh610/SfRh101 mixture, respectively. The more interesting plot is that of the Rh610/Rh640 mixture where there is clear evidence of periodic structure with a period of the order of 90 pixels in the spectra. This is witnessed by the clear peak in the auto-correlation function at a gap of 90 pixels. This structure was not present in either the Rh610 or the Rh640 spectra (see Fig. 6), but is present in the mixture. The Rh610/SfRh101 mixture does not display the same trends.

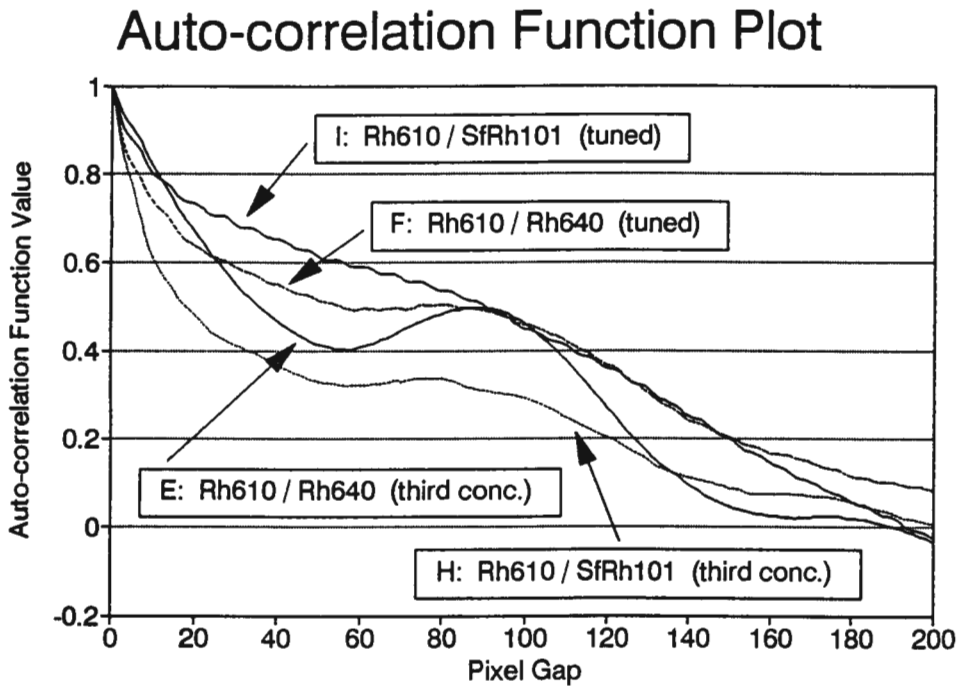

Figure 8: Dye spectra auto-correlations for Rh610/Rh640 and Rh610/SfRh101 using both tuning methods

Figure 8 shows the auto-correlation functions for **E**, **F**, **H**, and **I** which are dye laser runs where the amplifier has been tuned in two different ways (cf. Section 4.1) for the Rh610/SfRh101 and Rh610/Rh640 mixtures. The Rh610/Rh640 displays the same structure with a peak at a gap of around 90 pixels as when only the oscillator was used. This structure is more obvious for the $\frac{1}{3}$ concentation method than for the case where the amplifier was tuned. More interesting structure, with a period of the order of 5 pixels can be seen for the Rh610/SfRh101 (tuned) case. During the measurements, difficulty was experienced in tuning the amplifier to the correct wavelength and as a consequence a large amount of SfRh101 dye had to be added (cf. Table 2). It is possible that this is what distinguishes run **I** from the other runs and is the cause of the small-scale structure though the mechanism remains unknown.

Also interesting is that the method of $\frac{1}{3}$ concentration results in less mode correlation than the tuning method with the Rh610/SfRh101 ($\frac{1}{3}$ conc.) showing the least mode correlation of all. Results of Section 5.5 show that, as a general trend, a lesser degree of mode correlation results in a lower value for the spectral noise. For example, the Rh610/SfRh101 ($\frac{1}{3}$ conc.) is the least noisy of the four cases shown in Figure 8. Likewise, showing the same trend, the SfRh101 (osc. only) is the least noisy and Rh610 (osc. only) is the most noisy of the three cases shown in Figure 6. This same trend was observed for the June 1992 measurements.

Figure 9 shows the auto-correlation functions calculated from the non-resonant CARS spectra of runs **E-CARS**, **F-CARS**, **H-CARS**, and **I-CARS**. Periodic structure in the spectra is once again noticable for the Rh610/Rh640 ($\frac{1}{3}$ conc.) case, but this time the correlation period is of the order of 50 pixels. Taking the effect of the spectrometer dispersion at the different wavelengths into account, gives a correlation period of $\sim 0.51\ nm$ for the dye laser spectra and a period of $\sim 0.32\ nm$ for the non-resonant CARS spectra. The reason for this difference is not understood. From simple reasoning one might expect the non-resonant CARS spectra to follow the dye laser spectra. This does not appear to be the case for small-scale structure.

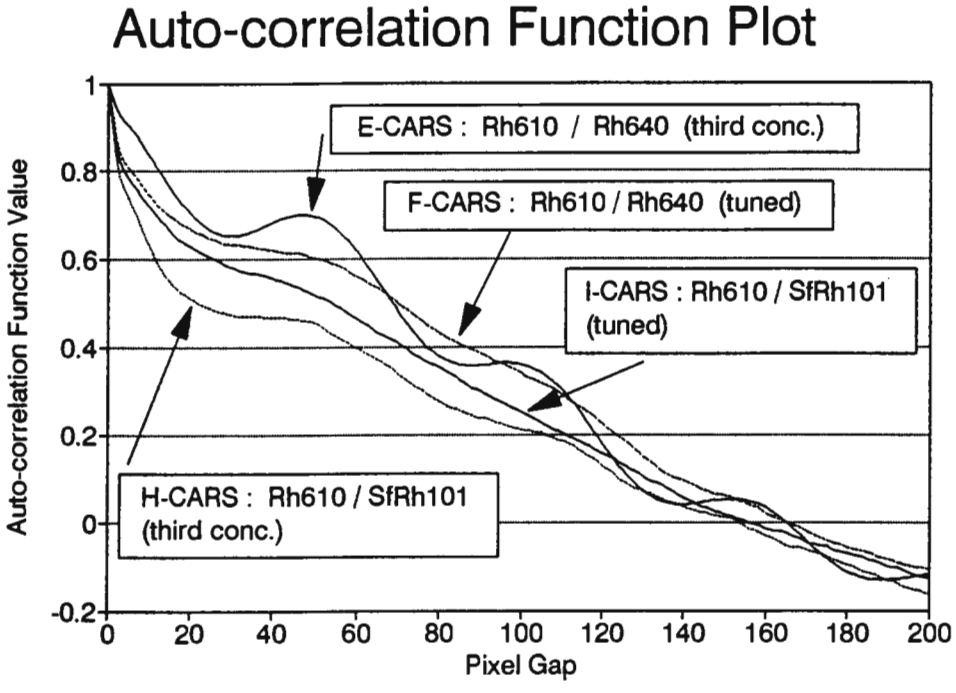

Figure 9: CARS spectra auto-correlations for Rh610/Rh640 and Rh610/SfRh101 using both tuning methods

5.5 Percentage Noise

Perhaps the most robust method of quantitively describing the noise in a spectrum is to express it as the ratio of the standard deviation to the mean for a particular pixel in the detector array and then to average over the detector pixels spanning the spectral region of interest. Use of this criterion permits relatively easy noise comparison between different laboratories and appears to be the most widely used method of quantifying noise in a spectrum [5] [14] [4] [3] [6] [1].

The finer details of the analysis such as the normalisation procedure used (if any) have varied from author to author. Two different methods have been investigated here and are outlined below.

5.5.1 Method A

A set of spectra recorded by the OMA can be expressed as $C_i^{(k)}$ where

$$\begin{aligned} C_i^{(k)} &= I_i^{(k)} D_i \\ i &= 1...\mathcal{P} \text{ pixels} \\ k &= 1...\mathcal{S} \text{ spectra} \end{aligned} \tag{24}$$

$I_i^{(k)}$ is the intensity of the light incident on detector pixel i for spectrum k and D_i is the sensitivity of detector pixel i. The detector pixels span the region of spectral interest and are numbered such that pixel 1 detects the photons with the lowest wavelengths in the region. For analysis of dye laser spectra, typically 100 pixels were discarded at each end of the detector array (1024 pixels) to remove instrument effects.

The removal of detector noise due to detector dark current and scattered light not originating from the laser beams has been discussed in Section 3.3.

For N_2 CARS, only the spectral profile is important and not the magnitude of the signal and so, for purposes of comparison, the spectra are first normalised to constant integrated energy. This is achieved by nomalising each pixel to produce a set of normalised spectra $N_i^{(k)}$ where

$$N_i^{(k)} \equiv \frac{C_i^{(k)}}{\sum_{i=1}^{\mathcal{P}} C_i^{(k)}} \tag{25}$$

An average normalised spectrum $\overline{N_i}$ is then found.

$$\overline{N_i} = \frac{\sum_{k=1}^{\mathcal{S}} N_i^{(k)}}{\mathcal{S}} \tag{26}$$

For each pixel, the standard deviation of the counts recorded by the pixel is then found where the sum is taken over the spectra.

$$\sigma_i = [\frac{\sum_{k=1}^{\mathcal{S}} (N_i^{(k)} - \overline{N_i})^2}{\mathcal{S}}]^{\frac{1}{2}} \tag{27}$$

The noise for the pixel, denoted by γ_i, and defined as the standard deviation divided by the average counts for that pixel, is then calculated.

$$\gamma_i \equiv \frac{\sigma_i}{\overline{N_i}} \tag{28}$$

Finally, the average noise for the set of spectra is calculated by averaging over the detector pixels.

$$\overline{\gamma_A} = \frac{\sum_{i=1}^{\mathcal{P}} \gamma_i}{\mathcal{P}} \tag{29}$$

5.5.2 Method B

The second method of noise characterization is similar to one used by Snelling et al. [5] [6] and Greenhalgh et al. [14] and is described below.

For this method, a set of spectra is represented in the same manner as given in Equation 24 for Method A.

The same normalisation procedure is used as for Method A to remove shot-to-shot energy fluctuations from the data :

$$N_i^{(k)} \equiv \frac{C_i^{(k)}}{\sum_i C_i^{(k)}} \tag{30}$$

An average normalised spectrum $\overline{N_i}$ is once again found for the set.

$$\overline{N_i} = \frac{\sum_{k=1}^{\mathcal{S}} N_i^{(k)}}{\mathcal{S}} \tag{31}$$

Normalised spectra are then divided by the average normalised spectrum to produce ratioed spectra $R_i^{(k)}$ where

$$R_i^{(k)} \equiv \frac{N_i^{(k)}}{\overline{N_i}} \tag{32}$$

$R_i^{(k)}$ is now independent of the detector pixel sensitivity D_i and represents shot-to-shot spectral fluctuations from the average spectrum.

The mean value of $R_i^{(k)}$ is then found for the spectrum.

$$\overline{R^{(k)}} = \frac{\sum_{i=1}^{\mathcal{P}} R_i^{(k)}}{\mathcal{P}} \tag{33}$$

The standard deviation of the ratioed spectrum from its mean value is then found.

$$\sigma_R^{(k)} = [\frac{\sum_{i=1}^{\mathcal{P}} (R_i^{(k)} - \overline{R_{(k)}})^2}{\mathcal{P}}]^{\frac{1}{2}} \tag{34}$$

The noise for the spectrum $\gamma_B^{(k)}$, defined as the standard deviation divided by the mean is then found.

$$\gamma_B^{(k)} \equiv \frac{\sigma_R^{(k)}}{\overline{R^{(k)}}} \tag{35}$$

Finally, the average noise for the set of spectra $\overline{\gamma_B}$ is found by averaging over the spectra.

$$\overline{\gamma_B} = \frac{\sum_{k=1}^{\mathcal{S}} \gamma_B^{(k)}}{\mathcal{S}} \tag{36}$$

Table 4: Comparison of noise quantifying methods

file	*edge*	noise A (%)	noise B (%)
Large Beads 1	100 (200)	6.9 (6.6)	6.8 (6.5)
Large Beads 2	100 (200)	7.5 (7.2)	7.5 (7.2)
No Beads 1	100 (200)	6.4 (6.2)	6.4 (6.2)
No Beads 2	100 (200)	6.4 (6.1)	6.5 (6.2)
Med. Beads 1	100 (200)	10.1 (9.1)	9.7 (8.9)
Med. Beads 2	100 (200)	10.4 (9.7)	10.2 (9.5)

5.5.3 Method Comparison

A comparison was made of Methods A and B, described in Sections 5.5.1 and 5.5.2, respectively. This was carried out by calculating noise values from June 1992 data for the two methods. The measured data comprised files containing sets of consecutive dye laser spectra (32 spectra in a file) recorded under varying conditions such as with and without beads in the oscillator (cf. Section 6).

The values obtained for the noise in each set of spectra using Methods A and B is given in Table 4. The "edge" parameter gives the number of pixels discarded at each end of the detector array. Noise figures in parentheses are the values when an edge of 200 pixels was used.

The noise figures of Table 4 show that while the two methods of analysis are not mathematically identical, they lead to very similar values for the noise. It has been noted in Reference [1] that noise defined according to Method B is a weak function of the analysis bandwidth. Table 4 shows that this is also also true for Method A. Thus it is reasonable to use either method, but for accurate noise comparisons with other laboratories it is necessary to make use of the same method of analysis and analysis bandwidth in each laboratory. It was decided to use Method A for the noise analysis in this thesis as this is the easier of the two to handle computationally when large data sets are being analysed.

5.5.4 Dye Laser Noise

In this section, noise values as calculated using Method A as described in Section 5.5.1 are presented. The noise figures in Table 5 are the averages over five files taken for each dye combination and the standard deviation of the mean σ_m reflects the fluctuations in the noise values between the files.

Table 5: Noise Figures for Dye Laser

letter code	*description*	*noise* (%)	σ_m (%)
A	Rh640 (osc. only)	9.7	0.2
B	SfRh101 (osc. only)	9.1	0.2
C	Rh610 (osc. only)	23.8	1.7
D	Rh610/Rh640 (osc. only)	20.1	0.8
E	Rh610/Rh640 ($\frac{1}{3}$ conc.)	22.5	0.7
E-CARS	non-resonant CARS using **E**	20.4	1.3
F	Rh610/Rh640 (tuned)	20.9	1.1
F-CARS	non-resonant CARS using **F**	14.8	0.8
G	Rh610/SfRh101 (osc. only)	18.6	0.9
H	Rh610/SfRh101 ($\frac{1}{3}$ conc.)	13.3	0.5
H-CARS	non-resonant CARS using **H**	10.2	0.5
I	Rh610/SfRh101 (tuned)	23.5	0.9
I-CARS	non-resonant CARS using **I**	15.4	0.5

The letter codes used are the same as found in Section 4.1.

As mentioned previously, preliminary results pointed to the Rh610 dye as being a major contibutor to spectral fluctuations. This is very clear from the runs using only the oscillator where the noise for the Rh610 (23.8%) is far greater than for the Rh640 (9.7%) or the SfRh101 (9.1%). This important result shows that a large portion of spectral noise is related to the intrinsic properties of the dye being used. It is unfortunate that in order to produce a satisfactory Stokes beam at 607 *nm* it is necessary to make use of the Rh610 dye, the most noisy of the three dyes investigated. As mentioned previously, the beam power using the SfRh101 dye on its own was not high enough at 607 *nm* to be satisfactory for CARS.

Runs **D** and **G** using only the dye laser oscillator show that the dye mixtures *are* less noisy (20.1% and 18.6%) than the Rh610 on its own, but not substantially so.

The results for the two methods of choosing concentrations for the dye laser amplifier for the Rh610/Rh640 dye, **E** and **F**, show that the method used is not a crucial factor determining spectral fluctuations. Noise figures for the Rh610/Rh640 with the amplifier in use are marginally higher than the noise figures for the case when only the dye oscillator, indicating that the dye amplifier does not contribute significantly to the noise.

On the other hand, the results for **H** and **I** seem to indicate that for the Rh610/SfRh101 mixture, the method of $\frac{1}{3}$ concentration produces signifi-

cantly less noisy spectra than the tuning method. This result should be treated with caution for two reasons :

1. As mentioned in Section 5.4.2, problems were experienced in tuning the amplifier to the correct wavelength and an 'unusually high' concentration of SfRh101 was needed in the amplifier. The amplifier emission peak was remarkably insensitive to the addition of extra SfRh101. This was not the case during the June 1992 measurements when a much lower relative concentration of SfRh101 was needed for the same tuning.

2. A repeat set of measurements of run **H** were taken a few days after the set presented in Table 5 for use as a comparison during the work with the latex beads (cf. Section 6). These measurements were taken as a double check in case there existed day-to-day variations in noise values from the same dye mixture. The noise figure calculated from these spectra was $20.7 \pm 0.6\%$. This is not consistent with the previous measurements. As the laser setup was identical for the two sets of measurements, the most plausible explanation is that the dye mixture is not chemically stable over long (of the order of days) periods and may not be stable over shorter periods.

Therefore, it is not unlikely that any small differences in noise values calculated from the different amplifier concentrations for the Rh610/SfRh101 mixture could be masked by the other effects described above. However, on the whole it appears that no great noise benefit is derived from using the method of tuning the amplifier. The method of using $\frac{1}{3}$ of the oscillator concentrations in the amplifier should be preferred as the spectra obtained seem less noisy and this method is the easier to implement.

It is interesting to note that the noise values for the non-resonant CARS spectra **E-CARS**, **F-CARS**, **H-CARS**, and **I-CARS**, are lower than the corresponding dye laser spectra, but generally follow the dye laser noise.

The limited (data aquisition problem) results from the June 1992 measurements indicated a much lower level of spectral noise than the most recent set. These results are much closer to the noise values that have been reported elsewhere [1] [3]. For example, the noise measured for Rh610 on its own using only the oscillator was of the order of 8.0%. The dye laser noise using the Rh610/Rh640 mixture was $\sim$ 6.0% and the noise using the Rh610/SfRh101 mixture was $\sim$ 5.5%. These noise values are all far lower than the present set and indicate that the Rh610 dye is the major cause of the discrepancy.

The preliminary measurements in May 1991 gave noise values of $\sim 30\%$ for the Rh610/Rh640 dye which is considerably more noisy than both the other measurement sets. Different batches of the Rh610 dye were used for the three sets of measurement. The noise results seem to indicate that the chemical properties of the dyes are a major factor in determining spectral fluctuations and that these properties can change over time and can vary from batch to batch. More investigation is needed in this area.

6 Scattering by Beads

The results of Section 5.4 have shown that there exist significant correlations between modes of the dye laser. It is reasonable to assume that if there were some method of suppressing mode correlations, the large shot-to-shot spectral fluctuations of the dye laser would be reduced. It was thought interesting to see the effect on the mode correlations when small latex beads were introduced into the oscillator cavity. The scattering of the laser light by these beads should scramble the phase structure of the modes and hence reduce mode correlations. The idea of inserting scattering objects into the dye laser oscillator was met with scepticism from quite a few sources as many people believed that the laser would cease to lase. This has been shown not to be the case.

6.1 Scattering Background

The presence of inhomogeneities in a medium causes the scattering of light. Light propagating through a perfectly homogenous medium is not scattered. Any material medium contains inhomogeneities in the form of molecules. However, for a crystal at absolute zero temperature, the regular arrangement of the molecules causes the scattered waves from each molecule to interfere in such a way as to produce no scattering at all, but only a change in the velocity of propagation.

For gases and fluids, the statistical fluctuations in the arrangement of the molecules can cause significant scattering. It is a difficult problem to develop a scattering theory which takes these statistical fluctuations into account as the phase relations between the waves scattered by neighbouring molecules must be studied in detail. This requires an accurate description of the interaction between molecules which can be very complicated. Problems of this sort are known as dependent scattering problems. An analysis of the scattering of light by the molecules of the dye solution within the dye cells of the dye laser is an extremely complicated problem as not only do statistical fluctuations of the fluid have to be taken into account, but the flow of dye solution through the cell is turbulent which introduces additional complications. Such an analysis is beyond the scope of this thesis.

Van de Hulst [28] defines *independent scattering* as the scattering of light by particles that are sufficiently far from each other that it is possible to study the scattering of one particle without reference to the other ones. A rough criterion for independent scattering is that the mutual separation between

particles is at least three times the scattering particle radius. This is true for most cases where alien bodies are immersed in the medium. Examples of this are dust particles in air and bubbles in water. This is also true for our case of the small latex beads in water and glycerine.

For independent scattering, there is no fixed phase relationship between waves scattered by different particles. Thus the scattered waves may interfere constructively or destructively or any possibility in between. Therefore, the intensities scattered by the various particles must be added without regard to phase for independent scattering [28].

For a non-absorbing dielectric material (such as a latex bead), the electrical conductivity is zero and the refractive index m is a real constant. The phase shift in radians for light passing along a diameter of such a sphere is given by [28]

$$\Delta\phi = 2a(m-1)\frac{2\pi}{\lambda} \tag{37}$$

where a is the radius of the sphere, m is the refractive index of the sphere measured relative to the surrounding medium, and λ is the wavelength of the light in the surrounding medium. This is the maximum phase shift associated with a single scattering. Smaller phase shifts occur for light not passing along a bead diameter. Therefore, the presence of the beads in the dye laser oscillator should result in there being randomly different phase shifts introduced for each mode and a corresponding reduction in mode correlation. It has been observed (cf. Section 5.4) that a higher degree of mode correlation results in a correspondingly larger noise value and thus noise should be reduced through the introduction of the beads.

6.2 Experimental Setup and Results

The effect of inserting a suspensions of three different sizes of latex beads into the dye laser oscillator was investigated. The technical name for the latex used is Styrene Divinylbenzene and the refractive index of the beads is 1.58. The three bead sizes were

- 2.0 μm diameter beads suspended in water
- 10 μm diameter beads suspended in water
- 173 μm diameter beads suspended in glycerine

Table 6: Phase shift after propagation along bead diameter

diameter (μm)	*phase shift* (radians)
2.0	5.23
10	26.2
173	185

The refractive index of the water was taken to be 1.33 and the refractive index of the glycerine was 1.47. Table 6 gives the phase shifts for light propagating along the bead diameter according to Equation 37 for the three bead suspensions.

A cell with transparent windows containing the bead suspensions was inserted into the dye laser oscillator. The cell was angled slightly to avoid auto-collimation effects. Spectra were obtained of the dye laser output with the three bead sizes. In addition, spectra were obtained for the 10 μm diameter beads and the 2 μm diameter using three different bead concentrations. The bead concentrations were measured with a Malvern Particle Sizer by observing obscurations. The obscuration measured for a particular bead concentration was the percentage of light scattered in a single pass through the cell. Only one concentration of the 173 μm diameter beads was investigated as, due to their large size, it was necessary to suspend these beads in glycerine rather than in water in which the beads sank to the bottom too quickly. It is very difficult to set up the Malvern Particle Sizer with glycerine and so the obscuration could not be measured. Hence, it was decided to use only one concentration of the larger beads.

The use of the beads was investigated with the Rh610/SfRh101 dye mixture using the same concentrations as for **H** (cf. Table 2).

It must be noted that these were exploratory measurements in order to obtain qualitative ideas about the effects of deliberately introducing scattering particles into a laser oscillator. Further investgation, covering a greater range of bead concentrations and and phase shifts introduced, is needed for a fuller understanding.

6.3 Noise Comparison

The noise figures for the bead runs can be found in Table 7. For the comparison run where no beads were used, a higher noise value was observed than for the corresponding run **H** of Section 5.5.4. This has been discussed in that section.

Table 7: Noise Figures for Dye Laser with Bead Suspensions

beads (μm)	*obscuration* (%)	*noise* (%)	σ_m (%)
no beads		20.7	0.6
2	20	16.2	0.2
2	50	16.4	0.2
2	75	17.9	0.2
10	20	17.2	0.4
10	47	16.7	0.2
10	75	19.3	0.6
173	$\sim$ 50 (estimated)	12.7	0.8

From the table, it is apparent that the introduction of the scattering particles into the dye laser oscillator does result in a small reduction of the spectral noise, but the effect is not dramatic. There appears to be little difference between the small and medium sized beads. Use of the large beads resulted in a larger noise reduction than the other beads (noise reduced from $20.7 \pm 0.6\%$ to $12.7 \pm 0.8\%$).

It is also clear that varying the bead concentration does not result in significant changes to the noise value. The results indicate that the use of a bead concentration corresponding to an obscuration of between 20% and 50% should give the best results. The higher bead concentrations (75% obscuration) proved to be the most noisy and were accompanied by a significant drop in beam power. This drop in beam power was also observed for the 20% and 50% obscuration cases, but was not as significant ($\sim$ 20% drop in power). Further investigation is needed on the effect that the insertion of the beads has on the beam power.

6.4 Auto-correlation Comparison

Figure 10 shows the auto-correlation functions for **H** and the reference run with no beads in which the run **H** concentrations were used. The term 'pixel gap' refers to the difference in correlated pixels, as before. As discussed previously, these two runs unexpectedly gave different noise values. The auto-correlation plot shows that while the general shape is preserved, there is a clear increase in correlations between groups of modes for the reference run. This also fits in with the general trend observed earlier that a greater degree of mode correlation accompanies an increase in spectral noise.

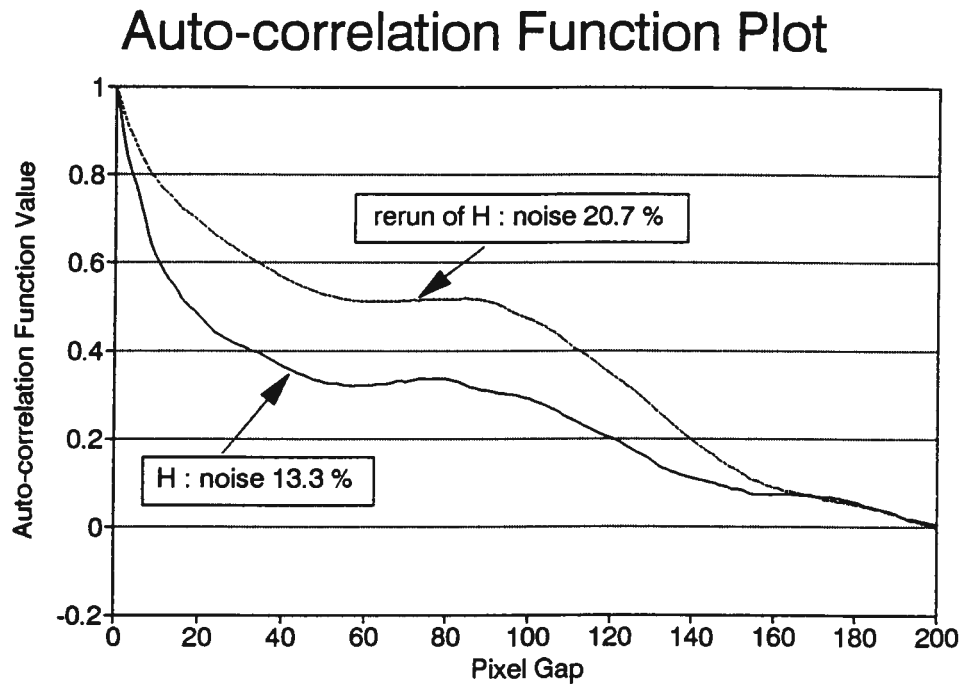

Figure 10: Dye spectra auto-correlations for Rh610/SfRh101 (third conc.) taken on different days.

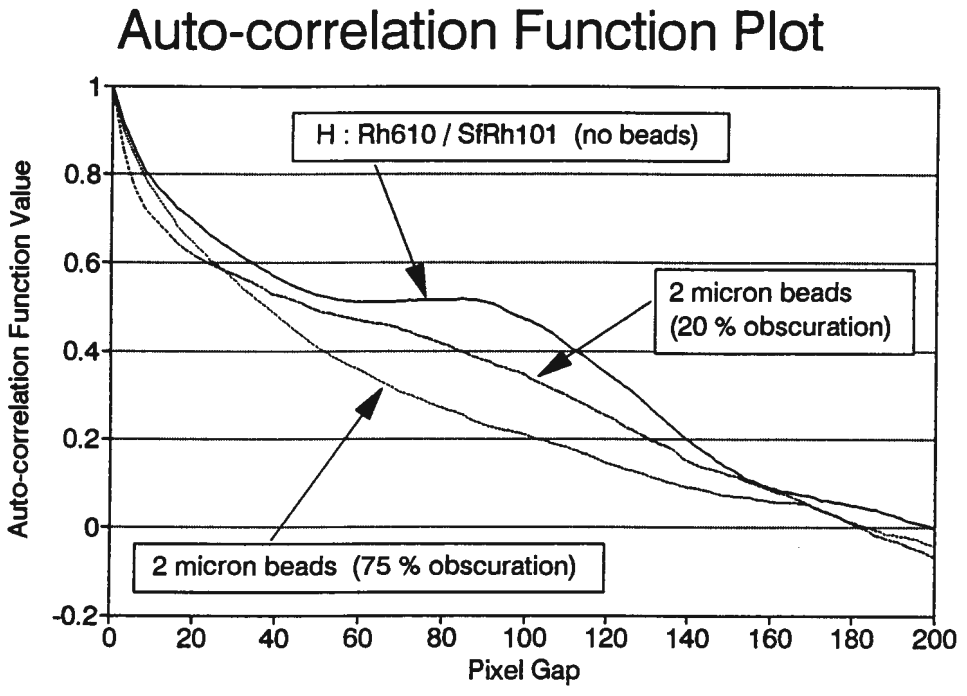

Figure 11: Dye spectra auto-correlations for 2 μm beads.

It was found that the auto-correlation functions for the 2 μm beads for obscurations of 20% and 50% were very similar. Shown in Figure 11 are the functions for the 2 μm beads for obscurations of 20% and 75% as well as for the reference case where no beads were used. The plot shows that the introduction of scattering particles into the dye laser oscillator does not remove all mode correlation, but does result in some smoothing in the auto-correlation function. In particular, the peak at a pixel gap of around 90 pixels is smoothed out.

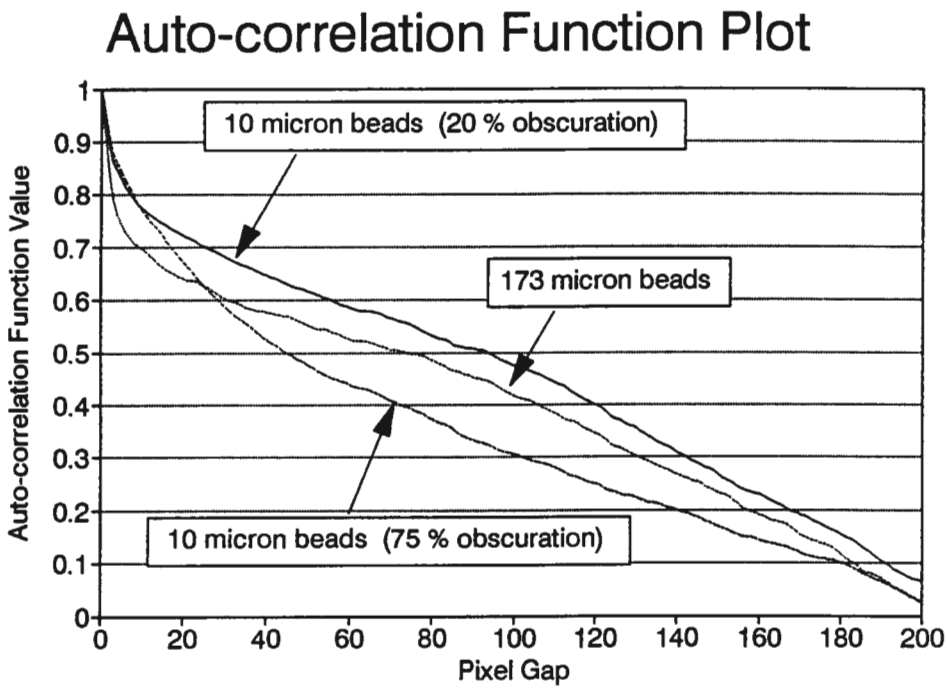

Figure 12: Dye spectra auto-correlations for the 10 μm beads and for the 173 μm beads.

Figure 12 shows the auto-correlation functions for the 10 μm beads at obscurations of 20% and 75% as well as that for the 173 μm beads. As was the case for the 2 μm beads, the auto-correlation functions for the 20% and 47% obscurations were very similar and hence the 47% obscuration case is not shown. In addition, as before, the presence of the beads results in a smoother auto-correlation function. Also noticable is the sharper initial drop-off for the 173 μm beads than for the 10 μm beads.

Thus the use of the scatterers in the dye laser oscillator has shown some promise as a method of noise reduction, but the improvement has not been dramatic. Use of the lower bead concentrations seemed to provide the best results and the use of the large bead size showed a significant improvement over the smaller sizes. There is much still to be understood and investigated in this area as the work presented here was only intended to be exploratory in nature.

7 Ti:Sapphire Laser

The poor noise performance of dye lasers has been observed for some time. As mentioned previously, turbulence in the dye flow has been listed as a possible cause of the spectral fluctuations [13]. Another factor possibly affecting noise performance of the dye laser is the presence of moving thermal gradients in the dye. A solid state laser should not suffer from these effects. A preliminary investigation of the noise characteristics of a tunable broadband $Ti : Al_2O_3$ laser has been carried out and is described in this section. This provides a useful comparison with the dye laser.

7.1 Ti:Sapphire Assembly and Setup

The $Ti : Al_2O_3$ laser was purchased from B.M. Industries and arrived in kit form. The laser is longitudinally pumped by the frequency-doubled Nd:YAG and is tuned by rotating a prism in the cavity. It was found that accurate positioning of the prism position was necesssary as a movement of the order of one degree moved the peak from 746 nm to 776 nm. The tuning prism was mounted on a rotating table which allowed fine movement through the use of a micrometer adjustment. The tunable range as given by the manufacturers extends from 690 nm to 880 nm. The layout of the laser is given in Figure 13. The tuning curve for the laser as supplied by the manufacturers is given in Figure 14.

The recording of the Ti:Sapphire spectra presented a few new problems as the spectrometer used was not designed for such long wavelengths. The holographic grating needed to be angled past its maximum position for the long wavelengths and as a result had to be repositioned in order that the light be directed onto the OMA detector pixels. The focussing telescope between the holographic grating and the detector pixels (cf. Figure 2) needed to be adjusted off the scale in its maximum position and a lens differing in focal length inserted in one side of the telescope in order to approach the correct focussing. A factor which prevented investigation of the output at wavelengths longer than $\sim$ 780 nm was that the detector pixels are blue-sensitised (ie. most sensitive to light at the CARS wavelengths) and the sensitivity drops off in the infra-red.

Care had to be taken not to use too high pump powers as a small spot was accidently burnt on the side of the crystal by focussing the pump beam too sharply. The threshold pump energy for operation of the Ti:Sapphire laser was found to be 25 $mJ/pulse$. Runs were taken at pump energies of

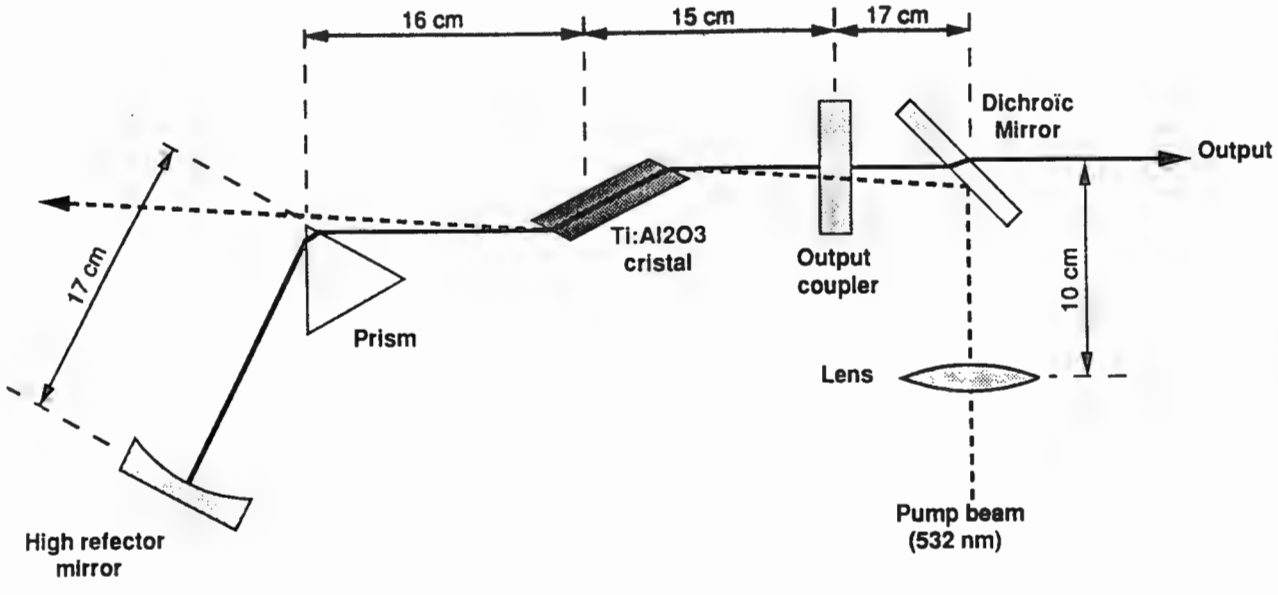

Optical configuration

Figure 13: Layout for Ti:Sapphire Laser

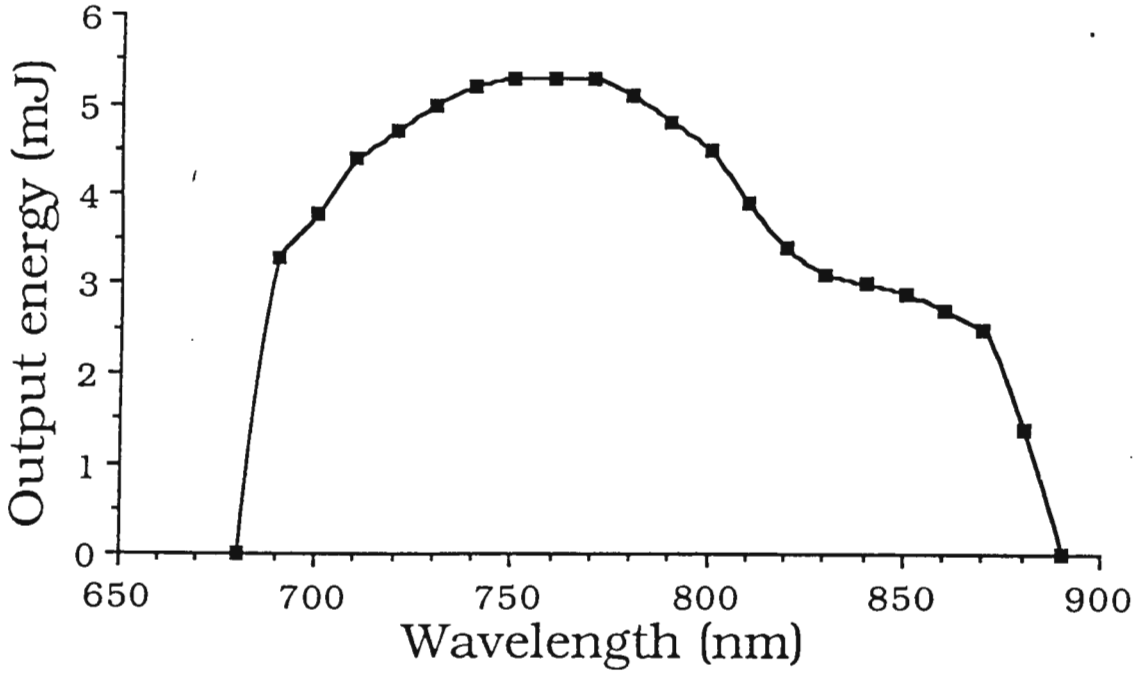

Figure 11: Tuning Curve for Ti:Sapphire Laser

38 $mJ/pulse$ giving a Ti:Sapphire output energy of $2.0 \pm 0.2\ mJ/pulse$. This was less than the manufacturers claim of an output energy of 5.3 $mJ/pulse$ with a pump energy of 23 $mJ/pulse$, but no serious attempt was made to optimise the Ti:Sapphire laser.

Two sets of runs were taken, one at 746 nm and the other at 776 nm. Each set consisted of 5 files of 50 shots. The laser repetition rate was 1 Hz.

7.2 Ti:Sapphire Results

Figures 15 and 16 show typical spectra obtained from the Ti:Sapphire laser at 746 nm and at 776 nm, respectively. Most striking is the differnce in spectral shape for the two plots with the spectrum at 776 nm having a much more pronounced tail. The FWHM value for the spectrum at 776 nm ($\sim$ 2.5 nm) is noticably larger than for the spectrum at 746 nm ($\sim$ 1.8 nm). A comparison with the dye laser spectrum of Figure 3 shows that the Ti:Sapphire laser emission is considerably narrower in bandwidth. However, the Ti:Sapphire laser is known to fluoresce over a large range of wavelengths (required for the tunability) and so a spectrally flatter output should be able to be produced by making suitable modifications to the laser cavity.

It was found that the wavelength of the peak shifted to longer wavelengths with increasing signal intensity. The maximum shift was of the order of 0.5 nm from the mean position. This is thought to be due to the characteristics of the gain curve and the spectral dependence of the mirror reflectivities. Fluctuations in the pump intensity result in a shift in the gain and the interaction between this and the frequency dependent losses due to the cavity mirrors is thought to cause the shifting of the spectral peaks. Mode-beating in the pump laser (occurs $\sim$ 5 % of the time) is one source of the energy fluctuations. It is likely that the peaks would not shift as much at higher pump powers. The laser was operated just above the lasing threshold as there was concern about damaging the crystal further with higher pump powers.

Shots whose total intensity was far removed from the mean intensity were once again removed as for the dye laser. In general, this resulted in more shots being removed ($\sim$ 15%) than for the dye laser ($\sim$ 8%).

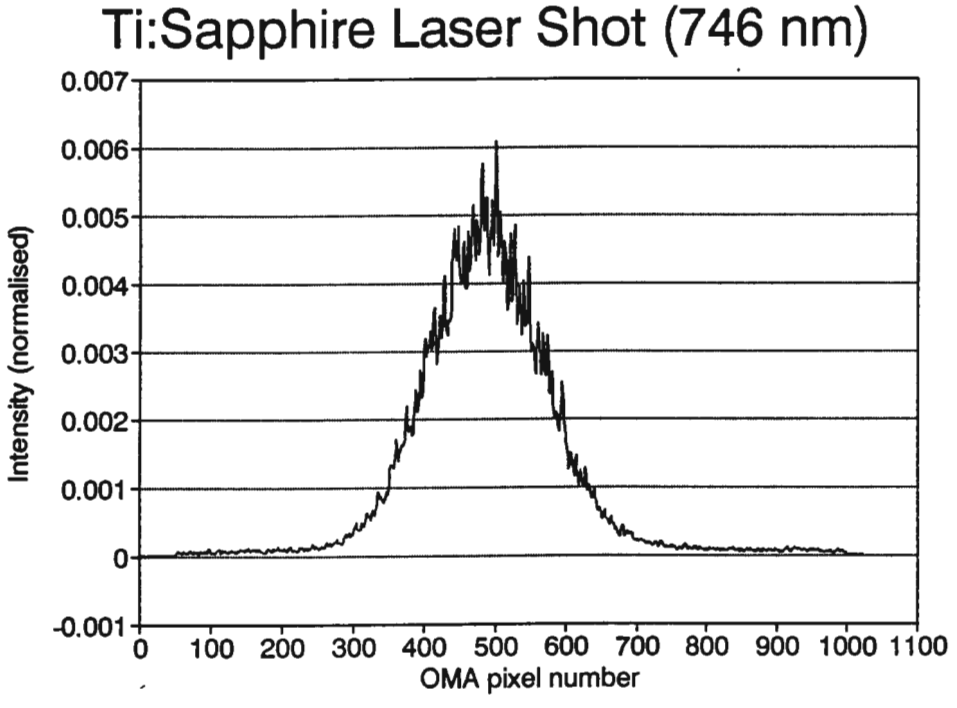

Figure 15: Typical Ti:Sapphire spectrum at 746 *nm*

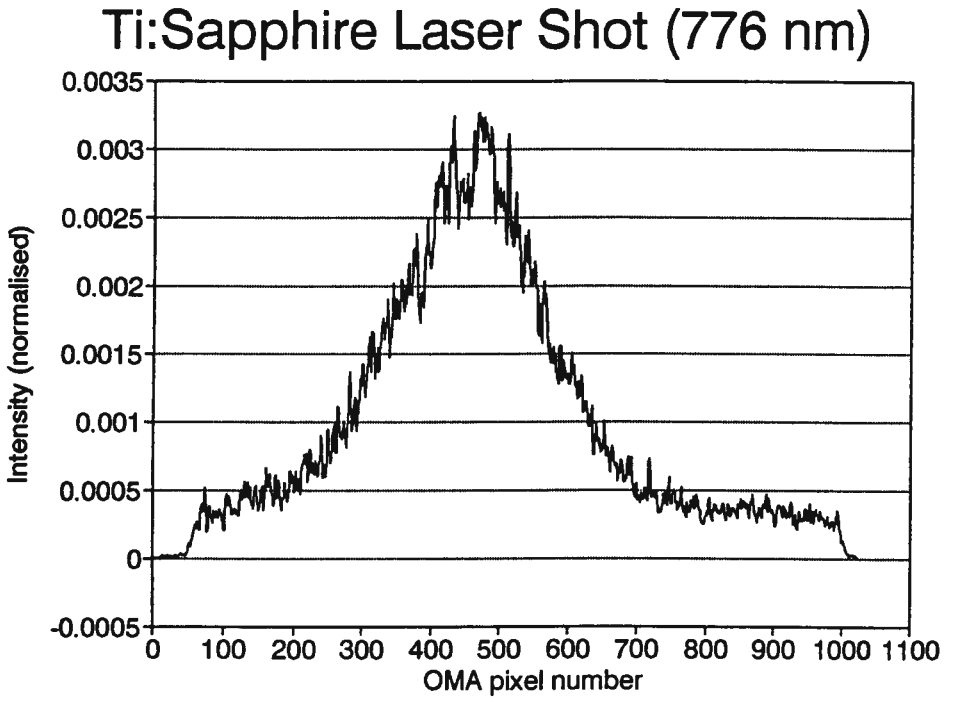

Figure 16: Typical Ti:Sapphire spectrum at 776 *nm*

Table 8: Ti:Sapphire Noise with Shifted Peaks

peak (nm)	*noise (%)*	σ_m (%)
746	44.2	5.1
776	23.3	1.4

7.2.1 Ti:Sapphire Noise

The noise was calculated in the same way as for the dye laser (cf. Section 5.5.1). Before the calculation, 100 pixels at each end of the OMA were discarded. The average of the noise over the five files is given in Table 8 for the laser tuned to 746 *nm* and to 776 *nm*.

The laser is noticably more noisy at the shorter wavelength and at first glance appears to be considerably more noisy than the dye laser. However, as has been mentioned, the wavelength of the peaks shifted according to signal intensity. It is likely that this effect is accentuated by running the laser just above threshold. The dye laser does not exhibit the same phenomenon and so for purposes of noise comparison, it is reasonable to remove this effect from the noise calculation. This is achieved by discarding those shots whose peaks are noticably displaced from the mean value. This was done for two files, one with the laser tuned to 746 *nm* and the other at the 776 *nm* tuning.

- File at 746 *nm*: 12 shots were discarded leaving 33 shots. This reduced the noise from 55.0 % to 25.5 %. The number of pixels discarded at each end of the OMA was 100. When 300 pixels were discarded at each end of the OMA the noise was maginally reduced to 25.0 %. This confirms that the analysis bandwidth is not a crucial factor in the noise calculation provided the the bandwidth is reasonably large.

- File at 776 *nm*: 17 shots were discarded leaving 33 shots. The noise was reduced from 21.1 % to 15.6 %. As a check that the reduced noise was not just a result of processing fewer shots, the first 33 shots in the file (with no shots discarded) were processed. This resulted in a noise figure of 21.2 % which is very close to the 21.1 % for the whole file (50 shots). Thus the processing of fewer shots does not on its own affect the noise figures provided a reasonable number of shots is processed (> 20).

After discarding the displaced shots, the noise figure of 15.6 % for the Ti:Sapphire laser tuned to 776 *nm* is comparable to the best noise figure

obtained for the dye laser (13.3 % for the Rh610/SfRh101 mixture cf. Section 5.5.4). The shorter wavelength noise figure of 25.5 % after discarding the displaced shots is comparable to the worst noise figures obtained from the dye laser (22.5 % for the Rh610/Rh640 mixture cf. Section 5.5.4).

It should be noted that the Ti:Sapphire results presented here should be regarded as preliminary in nature. These results represent the first spectra recorded from the newly-assembled laser. No serious attempt was made to optimise the laser output. On the other hand, noise in the dye laser output has been observed for some time and much work has been done to reduce the noise and optimise the system. In addition, significant day-to-day fluctuations in noise figures have been observed using the dye laser and it is thought that these arise from chemical instabilities in the dyes used (the Rh610 in particular). The Ti:Sapphire laser should not suffer from this effect and hence should prove easier to optimise.

It is clear that while the Ti:Sapphire laser does not represent the 'miracle cure' for broadband laser spectral noise, much more work is needed in optimising the laser before judgement can be made on whether this laser is a suitable replacement for the dye laser in CARS experiments.

7.2.2 Auto-correlation Analysis

Figure 7.2.2 shows the auto-correlation functions for the two files before and after discarding the displaced shots. The plot shows that the operation of discarding shots does not significantly alter the overall shape or small-scale structure of the auto-correlation functions, but results in apparently slightly reduced correlations. What is also clear from the plot is that, as in the dye laser, there exist significant correlations between groups of modes.

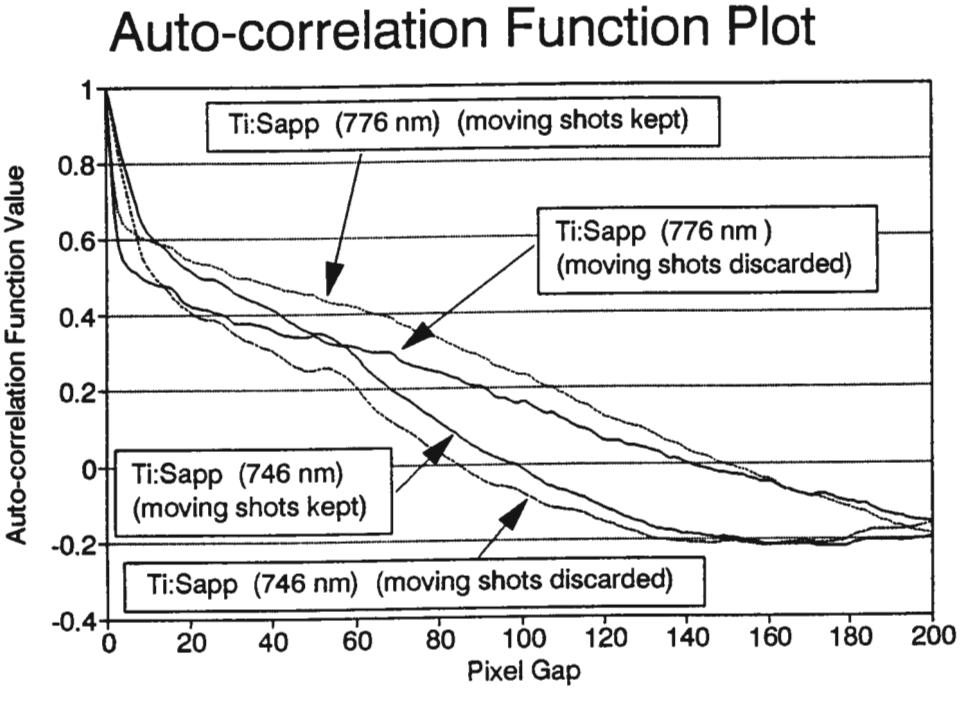

Figure 17: Auto-correlation Functions of Ti:Sapphire Spectra

8 Conclusions

A number of possible methods of characterizing noise in broadband dye laser spectra have been investigated. The failure of some of the standard statistical tests, such as the χ^2 test, in providing meaningful results has pointed to the existence of correlations between groups of modes in the dye laser. Methods of quantifying spectral noise reported in the literature have expressed the noise as the ratio of the standard deviation divided by the mean number of counts for each detector pixel. It was decided to use this method for noise characterization as it is reasonably robust and simple while allowing noise comparison with other laboratories.

A novel method of analysing correlations between modes using auto-correlation techniques, has been presented and has verified the existence of significant mode correlations in the dye laser. This is in contrast to a number of papers in the literature where the statistical independence of dye laser modes has been *assumed*. The degree of mode correlation has been shown to vary from dye to dye.

A comparison of dye laser spectral fluctuations using combinations of three dyes, Rh610, Rh640, and SfRh101, has been made. The dye laser emission peak was required at 607 *nm* for use as the Stokes beam in CARS experiments. Spectral noise has been shown to vary from dye to dye with the Rh610 dye proving to be considerably more noisy than the other two dyes. The least noisy dye was the SfRh101 which also displayed the least correlation between groups of modes. In fact this was observed as a general trend. A reduction in the degree of mode correlation was observed on the whole to accompany a reduction in spectral noise.

Two possible dye mixtures, Rh610/Rh640 and Rh610/SfRh101, have been investigated for use as the Stokes beam. It has proved necessary to persist with the Rh610 dye despite the poor noise performance, for want of a suitable substitute. The Rh610/SfRh101 mixture has proved less noisy than the Rh610/Rh640 mixture and should be preferred for use as the Stokes laser for CARS work.

Non-resonant CARS spectra from Argon have been shown to follow the shape of the dye laser spectra. The noise in non-resonant CARS spectra has been shown to follow the noise in the dye laser, but is slightly reduced. Thus it is important to reduce spectral fluctuations in the Stokes laser as much as possible.

A disconcerting feature of the dye laser noise analysis has been the large

variation in noise figures observed between sets of measurements taken at different times (a few months apart). It is thought that this is due to chemical differences between different batches of what is nominally the same dye. In this regard, the Rh610 dye has proved particularly unreliable and more investigation is needed in this area. In addition, lesser fluctuations in measurements of the Rh610/SfRh101 mixture taken days apart without altering the laser setup have also been observed and seem to point to chemical instabilities in the dye mixtures.

The large variations in the measurements taken months apart were originally thought to be a result of the different methods used to choose the concentrations for the dye amplifier. This has been shown to be not the case. The method of using one third of the oscillator concentrations in the amplifier shuold be preferred.

The effect of the deliberate insertion of scattering particles (latex beads in a liquid suspension) into the dye laser oscillator was investigated for the first time. Contrary to popular expectations, the laser continued to lase. The introduction of the beads did result in an improvement in in the spectral noise, but the improvement was not spectacular and significant mode correlations persisted. It was found that the lower bead concentrations provided the best results for the smaller beads. A more significant factor was the size of beads used with the large beads providing the best results. There is considerable scope for research in this area.

The results of the Ti:Sapphire laser measurements were slightly disappointing in nature. It was hoped that the Ti:Sapphire laser would prove to be the 'miracle cure' for spectral fluctuations. This has been shown not to be the case. The wavelength of the laser output was observed to shift with intensity. Even after removing this effect from the data, the spectral noise was of the same order as the dye laser with the longer wavelengths proving less noisy than the shorter wavelenghts. In addition, the spectral peak is significantly narrower than that of the dye laser though this could presumably be broadened by making suitable alterations to the Ti:Sapphire cavity. These Ti:Sapphire results should be regarded to be preliminary in nature as no work was done to optimise the laser. Much further work is needed in this area.

9 Acknowledgements

I would like to thank my two supervisors, Prof. G.N. Robertson and Dr H.S. Driver, for all their help and guidance during this MSc. I would also like to acknowledge the extensive assistance provided by Dr R.J. Hutcheon during the experimental measurements and thank J. Knight for help with the scattering beads and with the Ti:Sapphire laser. Thanks also to G. Morrison for fruitful discussions.

References

[1] D.R. Snelling, T. Parameswaran, and G.J. Smallwood. Noise characteristics of single-shot broadband CARS signals. *Applied Optics*, 26:4298–4302, 1987.

[2] M. Pealat, P. Bouchardy, M. Lefebvre, and J.-P. Taran. Precision of multiplex CARS temperature measurements. *Applied Optics*, 24:1012–1022, 1985.

[3] S. Kröll, M. Aldén, T. Berglind, and R.J. Hall. Noise characteristics of single shot broadband Raman-resonant CARS with single- and multimode lasers. *Applied Optics*, 26:1068–1073, 1987.

[4] R.J. Hall and D.A. Greenhalgh. Noise properties of single-pulse coherent anti-Stokes Raman spectroscopy with multimode pump sources. *J. Optical Society of America B*, 3:1637–1641, 1986.

[5] D.R. Snelling, R.A. Sawchuk, and R.A. Mueller. Single pulse CARS noise : a comparison between single-mode and multimode pump lasers. *Applied Optics*, 24:2771 -2778, 1985.

[6] D.R. Snelling, G.J. Smallwood, R.A. Sawchuk, and T. Parameswaran. Precision of multiplex CARS temperatures using both single-mode and multimode pump lasers. *Applied Optics*, 26:99–110, 1987.

[7] S.M. Curry, R. Cubeddu, and T.W. Hänsch. Intensity stabilization of dye laser radiation by saturated amplification. *Applied Physics*, 1:153–159, 1973.

[8] Z.W. Li, C. Radzewicz, and M.G. Raymer. Temporal smoothing of multimode dye-laser pulses. *Optics Letters*, 12:416–418, 1987.

[9] L.A. Westling, M.G. Raymer, and J.J. Snyder. Single-shot spectral measurements and mode correlations in a multimode pulsed dye laser. *J. Optical Society of America B*, 1:150–154, 1984.

[10] V.R. Mironenko and V.I. Yudson. Quantum noise in intracavity laser spectroscopy. *Optics Commun.*, 34:397–403, 1980.

[11] V.R. Mironenko and V.I. Yudson. Strong dependence of multimode laser generation spectrum on spatial localization of gain and losses. *Optics Commun.*, 41:126–130, 1982.

[12] G.M. Morrison. Backward Stimulated Raman Scattering. Master's thesis, University of Cape Town Physics Dept., 1993.

[13] T.H. Chyba, E.C. Gage, R. Gosh, P. Lett, and L. Mandel. Chaos in a good-cavity single-mode dye laser. *Optics Letters*, 12:422–424, 1987.

[14] D.A. Greenhalgh and S.T. Whittley. Mode noise in broadband CARS spectroscopy. *Applied Optics*, 24:907–913, 1985.

[15] L.A. Westling and M.G. Raymer. Intensity autocorrelation measurements and spontaneous fm phase locking in a multimode pulsed dye laser. *J. Optical Society of America B*, 3:911–917, 1986.

[16] H. Statz and C.L. Tang. Phase locking of modes in lasers. *J. Applied Physics*, 36:3923–3927, 1965.

[17] L.A. Westling, M.G. Raymer, M.G. Sceats, and D.F. Coker. Observation of intensity fluctuations and mode correlations in a broadband cw dye laser. *Optics Commun.*, 47:212–217, 1983.

[18] H. Atmanspacher and H. Scheingraber. Deterministic chaos and dynamical instabilities in a multimode cw dye laser. *Physical Review A*, 34:253-263, 1986.

[19] L.A. Kotomtseva, N.A. Loiko, and A.M. Samson. Instabilities leading to self-pulsing, hysteresis, and chaos in a multimode laser. *J. Optical Society of America B*, 2:232–235, 1985.

[20] H. Atmanspacher, H. Scheingraber, and C.R. Vidal. Mode-correlation times and dynamic instabilities in a multimode cw dye laser. *Physical Review A*, 33:1052–1059, 1986.

[21] S.A.J. Druet and J.P. Taran. CARS spectroscopy. *Prog. Quantum Electron.*, 7, 1981.

[22] R.J. Hall and A.C. Eckbreth. *Coherent Anti-Stokes Raman Spectroscopy (CARS): Application to Combustion Diagnostics*, volume 5 of *Laser Applications*. Academic, New York, 1984.

[23] J.W. Nibler and G.V. Knighten. *Coherent Anti-Stokes Raman Spectroscopy*. Raman Spectroscopy of Gases and Liquids. Springer, Berlin, 1979.

[24] A.V. Masalov. *Spectral and temporal fluctuations of broad-band laser radiation*. Progress in Optics XXII. Elsevier Science Publishers, 1985.

[25] T.U. Arslanbekov, N.B. Delone, A.V. Masalov, S.S. Todirashku, and A.G. Fainshtein. *Sov. Phys. JETP*, 45, 1977.

[26] Société de Production et de Recherches Appliquées. CARS issues. Technical report, SOPRA, April 1989.

[27] F.T. Arecchi and E.O. Schulz-Dubois, editors. *Laser Handbook*, volume 1, 387–389, North-Holland, 1972.

[28] H.C. van de Hulst. *Light Scattering by Small Particles*. John Wiley & Sons, 1957.